Cytonemes coordinate asymmetric signaling and organization in the *Drosophila* muscle progenitor niche

Akshay Patel[1], Yicong Wu[2], Xiaofei Han[2], Yijun Su[2,3], Tim Maugel[4], Hari Shroff[2,3], Sougata Roy[1*]

[1] Department of Cell Biology and Molecular Genetics, University of Maryland, College Park, Maryland, USA

[2] Laboratory of High-Resolution Optical Imaging, National Institute of Biomedical Imaging and Bioengineering, National Institutes of Health, Bethesda, Maryland, USA

[3] Advanced Imaging and Microscopy Resource, National Institutes of Health, Bethesda, Maryland, USA

[4] Department of Biology, Laboratory for Biological Ultrastructure, University of Maryland, College Park, Maryland, USA

* Correspondence: sougata@umd.edu

Running Title: Cytonemes asymmetrically pattern stem cells

Keywords: Cytonemes, polarity, synapse, stem-cell, niche, FGF, Heartless, Pyramus, Thisbe

ABSTRACT

Asymmetric signaling and organization in the stem-cell niche determine stem-cell fates. We investigated the basis of asymmetric signaling and stem-cell organization using the *Drosophila* wing-disc that creates an adult muscle progenitor (AMP) niche. We uncovered that AMPs extend polarized cytonemes to contact the disc epithelial junctions and adhere themselves to the disc/niche. Niche-adhering cytonemes localize an FGF-receptor to selectively adhere to the FGF-producing disc and receive FGFs in a contact-dependent manner. Activation of FGF-signaling in AMPs, in turn, reinforces disc-specific cytoneme polarity/adhesion, which maintains their disc-proximal positions. The wing-disc produces two FGFs in distinct zones and restricts their signaling only through cytonemes. Consequently, although both FGFs use the same receptor, their cytoneme-mediated signaling asymmetrically distributes different muscle-specific AMPs into different FGF-producing niches. Loss of cytoneme-mediated adhesion and FGF-signaling promotes AMPs to lose niche occupancy, occupy a disc-distal position, and acquire morphological hallmarks of differentiation. Thus, cytonemes are essential for asymmetric signaling and niche-specific AMP organization.

INTRODUCTION

Tissue development and homeostasis rely on the ability of stem cells to maintain a balance between self-renewal and differentiation. Stem cell fate decisions are made in the context of the niche that they adhere to and are controlled by asymmetric signaling and the physical organization in the stem cell microenvironment [1-9]. Asymmetric signaling maintains stem cell identity in niche-resident stem cells but promotes differentiation of their daughters outside the niche in an organized pattern. Physical organization and interactions between stem and supporting cells also control stem cell niche-occupancy and asymmetric signaling [1,10]. Understanding how asymmetric signaling and cellular organization arise and are coordinated within the stem cell microenvironment is critical to understand how stem cells maintain their identity and prime differentiation in an organized pattern to generate tissues.

Niche cells are known to present self-renewal growth factors to the stem cells in an asymmetric manner. Although these secreted signals can act over a long range and are predicted to disperse randomly in the extracellular environment, their activities are spatially confined to the niche. Moreover, signals are selectively distributed only to the stem cells, but not to their neighboring non-stem cell daughters, often located one cell diameter away [11,12]. Elegant experiments using cultured embryonic stem cells (ESC) have shown that asymmetric signaling and cell division require localized target-specific signal presentation [13]. For instance, while the spatially restricted presentation of bead-immobilized Wnt induces asymmetric cell division and signaling, the presentation of soluble Wnt and global activation of signaling in ESC sustains only symmetrical division [13]. These findings suggested that the localized and directed signal presentation and interpretation could form the basis of the asymmetry within the stem cell niche.

An in vivo mechanism for localized and directed distribution of signals during animal development came from the discovery of specialized signaling filopodia, called cytonemes [14-16]. Studies in developing *Drosophila* and vertebrate embryos demonstrated that signal-exchanging cells extend cytonemes to contact each other and

exchange signaling proteins at their contact sites [14,15,17-22]. Cytonemes have been implicated in all major signaling pathways [23-25]. Cytonemes or cytoneme-like signaling projections such as MT-nanotubes are known to be required in *Drosophila* germline stem cells niches [12,26,27] and stem-cell-derived synthetic organoids [28]. These previous observations raise the possibility that contact-dependent signaling through cytonemes could form the basis of asymmetric signaling and cellular organization in stem cell niches. However, much needs to be learned about the roles and mechanisms of cytonemes in establishing functional asymmetry in the stem cell niche.

To address this question, we selected the *Drosophila* wing disc-associated adult muscle precursors (AMPs), which constitute a well-characterized population of stem cells maintained within the wing disc niche [29,30]. AMPs are embryonic in origin and are associated with the larval wing disc to proliferate and produce a pool of transient amplifying cells that undergo subsequent myogenic fusions and differentiation to form adult flight muscles [29,31-34]. The wing imaginal disc produces several self-renewal signals for AMPs [30,34,35]. Disc-derived Wingless (Wg) and Serrate (Ser) cause asymmetric AMP divisions, which retain mitotically active AMPs at the disc-proximal space and place their daughters at a disc-distal location to commit to post-mitotic fates [30]. AMPs are also known to employ cytonemes to mediate Notch and Wingless/Wg (Wnt) signaling with the disc-associated trachea and wing discs, respectively [36,37]. These prior characterizations and the availability of genetic tools and imaging methods provide an ideal system to examine the roles of cytonemes in generating functional asymmetry in the wing disc AMP niche.

In this study, we showed that cytonemes are required to generate and coordinate asymmetric signaling and AMP organization within the wing disc niche. Investigation into the underlying mechanisms revealed the existence of a central self-regulatory mechanism involving cytoneme-mediated adherence and Fibroblast Growth Factor (FGF) signaling between AMPs and niche cells. In this mechanism, AMPs extend polarized FGFR-containing cytonemes to physically adhere to the FGF-producing wing disc and concomitantly receive FGFs from the disc in a contact-dependent manner.

Activation of FGF signaling in AMPs, in response, reinforces the polarity and selective adherence of cytonemes to the niche. We showed that these self-regulated niche-stem cell interactions through cytonemes maintain the niche-specific polarity, positional identity, and FGF signaling in the niche-adhering AMPs. These features are gradually lost in disc-distal AMPs due to the loss of the cytoneme-mediated niche adherence. Consequently, asymmetric signaling and AMP organization patterns emerge in coordination with each other. Furthermore, we showed that the wing disc niche controls the self-regulatory pathway in AMPs by expressing two different FGFs in distinct spatial zones and communicating them through cytonemes in a polarized and target-specific manner to shape diverse asymmetric patterns. These findings suggest that contact-dependent polarized signaling through cytonemes forms the basis of the signaling asymmetry and cellular organization in the stem cell niche.

RESULTS

AMP polarity changes with increasing distance from the wing disc niche.

In the 3rd instar larva, AMPs localize within a multi-stratified layer and are associated with the basal surface of the wing disc epithelium and disc-associated tracheal transverse connective (TC) and air-sac primordium (ASP) [30,38] (Fig. 1A). To gain insights into the cellular organization in the AMP niche, we examined wing discs using transmission electron microscopy (TEM) and confocal microscopy. TEM analyses of 16 wing disc (from w^{1118} larvae) sections revealed that AMPs asymmetrically organize orthogonally over the disc within a space between the basal surface of disc cells and the disc basal lamina (Fig. 1A-D). We identified two asymmetric features in the AMP organization along the proximo (p)-distal (d) orthogonal axis relative to the disc.

Firstly, most AMPs and AMP nuclei had polarized elliptical morphologies, but their orientation changed with the changes in AMP locations along the proximo (p)-distal (d) orthogonal axis, relative to the disc (Fig. 1A-D). While the disc-proximal (p) AMPs or AMP nuclei had their major axes oriented in the oblique-to-orthogonal direction relative to the disc plane, the disc-distal (d) AMPs/AMP nuclei had their major axes aligned parallel to the disc plane (Fig. 1B-C). Secondly, we found that the disc-proximal AMPs

(p) established direct membrane contacts with underlying disc cells and often extended projections (Fig 1B-D), similar to cytonemes [37], that protruded into the disc cell membrane or the intercellular space (Figs. 1D, S1A,A'). In contrast, disc-distal AMPs (d) lacked such direct physical contacts with the disc (Fig. 1B,C). These results indicated that the positioning of individual AMPs within the wing disc niche might be linked to their polarity and contact-dependent interactions with the disc.

To further verify the correlation between AMP polarity and positioning, we labeled AMP nuclei with nls:GFP (nuclear-localized GFP expressed under the AMP-specific *htl-Gal4* driver), and used confocal microscopy to record nuclear position and orientation in three dimensions, relative to the disc-AMP interface (phalloidin-marked) (Fig. 1E-F''). Nuclear labelling allowed us to distinguish relative locations and polarity of each AMP using YZ orthogonal sections relative to the discs (Fig, 1A,E-E''). To examine how nuclear polarity changed with increasing distance from the disc, we measured the angle between the wing disc plane and the major axis of each elliptical nucleus positioned at various distances away from the disc (n = 30 discs; Fig. 1G). With these analyses, we confirmed that disc-proximal AMP nuclei were polarized toward the disc, and disc-distal nuclei had their axes aligned parallel to the disc plane. Moreover, the polarity of AMP nuclei gradually changed with the increased orthogonal distance from the disc (Fig. 1E-H; Table S1).

In addition, as nls:GFP labeled both the nucleus and cytoplasm, these experiments also revealed diverse morphological features of distal AMPs. A population of *htl* expressing distal cells had small non-polar spherical (diameter ~2-5 μm) shapes. Another group of AMPs had highly elongated multi-nucleated (2-3 nuclei/cell) syncytial morphology, which is a hallmark of myogenic fusion [39] (Figs. 1I-K; S1B-D'). Notably, AMPs with diverse morphologies were predominantly enriched proximal to the TC and ASP and often adhered to the TC/ASP surfaces (Fig. S1C). It is possible that the disc-associated tracheal epithelium acts as a second niche to support disc-distal AMPs, but, here, we focus only on the disc-AMP interactions.

Disc-specific AMP polarity and positioning are linked to disc-adhering AMP cytonemes.

The appearance of morphologic features of fusion in disc-distal AMPs is consistent with the post-mitotic fates of the distal AMPs, as reported before [30,38]. Therefore, we hypothesized that the disc-specific AMP polarity and adherence maintain disc-proximal positional identity and stemness of AMPs, and that the loss of disc-specific polarity and adhesion enables AMPs to acquire disc-distal positions and morphologic features required for fusion/differentiation. To test this model, we generated a transgenic fly harboring a *htl>FRT-stop-FRT>Gal4* construct that can induce random fluorescently marked FLIP-out clones exclusively in the AMP layers (Figs. 2A; see Methods). Generation of sparsely located single-cell AMP clones, marked with either membrane-localized CD8:GFP or actin-binding Lifeact:GFP, allowed us to compare the morphologic features of AMPs present at different locations within the same tissue (Figs. 2B-B"; S1E,F).

Confocal YZ sections of discs revealed that disc-proximal AMPs (single cell clones) were oriented toward the disc, and they also projected long orthogonally-polarized cytonemes toward the disc that apparently invaded into the disc epithelium (~2-3/cell; ~12-15 μm long; Fig. 2B-B", Table S2). In contrast, the disc-distal AMP clones had diverse polar and non-polar morphologies and they appeared to adhere to each other, often forming syncytial morphologies (Figs. 2B", S1G-G'). Importantly, the polarized disc-distal AMPs had their axes aligned in parallel to the disc plane, as observed before, and although they extended laterally oriented cytonemes (av. ~ 6/cell) toward each other and the TC/ASP, they lacked orthogonal cytonemes (Fig 2B-B", Table S2). Notably, despite having morphologic hallmarks of AMP-AMP adhesion/fusion, distal AMPs (except for non-polar AMPs) still retained a promyogenic transcriptional state based on the expression of the transcription factor Twist (Twi) (Fig. S1H-H") [40]. These observations were consistent with the model that the loss of disc-specific polarity and adhesion primes AMPs to prepare for myogenic fusion.

The presence of orthogonally polarized disc-invading cytonemes exclusively in the disc-proximal AMPs suggested that these cytonemes might be involved in physically adhering/holding AMPs to the disc-proximal position and establishing their disc-specific polarity. Orthogonal AMP cytonemes appeared to be stable structures as they were detected in comparable numbers under both fixed and live conditions and irrespective of the genetic markers or drives used (Figs. 2C-E). Moreover, wing disc cells were also observed to extend short actin-rich projections, probably to promote AMP-disc physical interactions (Fig. 3F).

Further characterization of AMP cytonemes revealed that they are primarily composed of actin. AMP cytonemes were enriched with actin-binding phalloidin and Lifeact:GFP, but they lacked microtubule marker, such as EB1:GFP (Fig.S2A,A'). Live imaging of CD2:GFP-marked AMPs in ex-vivo cultured wing discs, revealed that the orthogonal cytonemes dynamically extend and retract at an average rate of ~ 1 μm/min and have an average life-time of ~ 25 min (Figs. 2G,H; S2C, Movies S1-S3; Table 3). Despite the regular turnover, the overall cytoneme density (niche occupancy) within the disc area remained uniform over time (Fig 2I,J; Movie S4). These results suggested that the AMPs are dynamically adhered to the disc via cytonemes and that this dynamism might enable multiple proximal AMPs to share the limited niche space.

AMP cytonemes anchor AMPs to the disc adherens junction.

To characterize the cytoneme-disc interactions, we simultaneously expressed CD2:GFP in AMPs under *htl-LexA* and nls:mCherry in the disc notum under *ths-Gal4* control. For deep tissue imaging of cytonemes (50-80 μm deep from the objective), we employed a triple-view line-confocal imaging method, which enabled ~2-fold improvement in axial resolution (Fig 3A-C) [41]. The orthogonal cytonemes were found to emanate in a polarized manner from only the ventral surface of disc-proximal AMPs and invade through the intercellular space of the disc epithelium (Fig. 3C-D''', Movie S5). Analyses of XY and XZ optical sections revealed that multiple AMP cytonemes shared a common disc intercellular space and they grew toward apical junctions of the disc epithelium (Fig. 3D-D'').

To examine if AMP cytonemes are tethered to the intercellular disc space, we expressed mCherryCAAX in disc cells and CD2:GFP in AMPs and imaged these tissues with an Airyscan confocal microscope. We also immunoprobed these tissues for various sub-apical adherens junction markers, including Discs-large protein, beta-catenin (Armadillo), and DE-Cadherin. As shown in Figure 3E-J (Movies S6, S7), long AMP cytonemes extended through the basolateral intercellular space of the wing disc cells and appeared to contact the sub-apical adherens junction (Fig. 3E-E'', G-H', Movie S7). Cytoneme tips are often helically twisted around the junctional membrane components (Fig. 3J), potentially to increase the surface area of the contacts.

To examine if AMP cytonemes selectively contact the apical disc junctions, we used the synaptobrevin-GRASP, a trans-synaptic GFP complementation technique (Methods) [20,42]. When we expressed CD4:GFP^{11} on the wing-disc cell membrane and mCherryCAAX and syb:CD4:GFP$^{1-10}$ in AMPs, high levels of GFP reconstitution occurred selectively at the contact sites between the tips of the cytonemes and the actin-rich (phalloidin-marked) disc apical junctions. Thus, AMP cytonemes establish direct contact with the disc adherens junctions (Fig. 3K,K'). It is important to note that although these experiments were performed using a disc-specific *ths-Gal4* driver, contacts between cytonemes and disc junction were recorded even in the AMP-occupied disc areas that did not express *ths-Gal4* (Fig 3H,H'). Thus, AMPs employ cytonemes to occupy the wing disc niche and this cytoneme-mediated occupancy is likely to be a general mechanism for AMP-niche adhesive interactions.

Cytoneme-disc contacts predict positional identity and polarity of AMPs relative to the disc.

If cytoneme-mediated adhesion is required to specify disc-specific AMP polarity, disc-proximal location, and stemness, removal of cytonemes might induce the loss of AMP polarity and niche occupancy and gain of distal positioning and fusogenic AMP-AMP adherence. The *Drosophila* Formin Diaphanous (Dia) is a known cytoneme modulator of actin-based cytonemes [15,36]. We found that AMP cytonemes localized Dia:GFP and a

constitutively active Dia^{act}:GFP (Fig. 4A-D). Moreover, compared to control discs, *dia* knockdown in Lifeact:GFP-marked AMPs significantly reduced AMP cytoneme numbers (Fig. 4A-D). Therefore, to record the effects of cytoneme loss in AMPs, we genetically removed AMP cytonemes by knocking down *dia* from AMPs. When *dia-i* was expressed in either Lifeact:GFP-marked (detects morphology) or nls:GFP-marked (detects nuclear polarity and number) AMPs under the *htl-Gal4* control, the number of AMPs and orthogonal AMP layers reduced significantly in comparison to the control (Fig 4E-I').

The remaining disc-resident mutant AMPs lost their disc-specific polarity and apparently fused to each other to acquire giant syncytial shapes (Figs. 4F; S3A). Cross-sections through these giant cells/chambers revealed that each one of them was lined by a common thick actin-rich membrane cortex (marked with phalloidin or Lifeact:GFP) housing multiple large-sized nuclei (probed with nls:GFP expression, DAPI and Twist-staining) (Fig.4F-G', I-I'). Assembly of multiple AMPs/AMP nuclei into the common chambers lined by Lifeact:GFP, which was expressed only in AMPs, indicated AMP-AMP adhesion and fusion. The reduction of AMP numbers and concomitant formation of giant AMP nuclei also suggested induction of growth, probably by suppressing cell division. Despite the induction of AMP fusion and morphological changes, syncytial AMP nuclei localized the promyogenic transcription factor Twi, as observed before (Fig. 4G). Thus, the loss of AMP cytonemes led to the loss of AMP polarity and instead facilitated fusogenic responses in AMPs.

To further determine if cytonemes are required for both maintaining AMP polarity/niche occupancy and inhibiting fusion, we generated Lifeact:GFP-marked single-cell AMP clones expressing *dia-i*. In comparison to control clones, *dia* mutant clones had non-polar spherical shapes, and lacked cytonemes (Fig. 4J-O). Importantly, while WT AMP clones occurred at random positions along the orthogonal p-d axis, cytoneme-deficient clones occurred only in the distal-most AMP layers (Fig. 4J-L'). Cross-sections through these non-polar clones revealed their syncytial nature (2-4 nuclei/cell) (Fig. 4M). Many small mutant cells also adhered to each other, forming actin-rich synapses, similar to those observed during myoblast fusions [43] (Fig. 4M, N-O). These results provided

evidence that polarized disc-adhering AMP cytonemes are required to predict disc-proximal AMP position, and that the lack of these cytonemes induces AMPs to acquire disc-distal positions and morphologic hallmarks of a fusogenic response.

AMP cytonemes polarize toward the disc by activating FGF signaling.

Disc-adhering cytonemes might also be required for contact-dependent reception of growth factors produced in the disc, and the activation of signaling, in turn, might specify the disc-specific polarity and fates in AMPs. The crosstalk between Wg/Wingless and FGF/Heartless (Htl) signaling pathways is known to control AMP multiplication [34,35,44]. The wing disc is known to produce Wg and the Htl ligand, Thisbe/Ths [34,35,44]. Therefore, we examined if orthogonal cytonemes localized the Wg receptor, Frizzled (Fz), and the Ths receptor, Htl, by expressing Fz:mCherry [36] and Htl:mCherry in CD2:GFP-marked AMPs. While 100% of the AMP cytoneme population localized Htl:mCherry, Fz:mCherry was present only on ~24% of the cytoneme population (Fig. 5A-C). A *htl:GFP*^{fTRG} fly line that expresses physiological levels of Htl:GFP [45], also localized Htl:GFP on the entire population of orthogonal cytonemes (Fig. 5D; Movie S8). Therefore, we hypothesized that cytonemes might be required for Htl signaling and that the cytoneme-mediated Htl signaling is common to all AMPs.

To detect the Htl-induced MAPK signaling in AMPs, we probed for nuclear dpERK. Most AMPs with nuclear dpERK were asymmetrically enriched at the disc-proximal locations (Fig. 5E). This asymmetric distribution of Htl signaling also correlated with the observed asymmetric p-d distribution of orthogonal AMP cytonemes (Fig. 2A,B). To examine if orthogonal cytonemes in disc-proximal AMPs were required to induce Htl signaling, we generated CD8:RFP-marked *dia-i* expressing clones of AMPs and probed for dpERK. In the control, 100% of the WT clones in the disc-proximal location (n = 24 from 3 discs) had dpERK (Fig. 5F-F''). By contrast, all of the cytoneme-deficient *dia-i* clones localized only in the distal layer and lacked nuclear dpERK (n= 48 clones, 7 discs) (Fig. 5G,G'). Thus, disc-adhering orthogonal cytonemes are required for Htl signaling.

To examine if the activation of Htl signaling is also required for the disc-specific orientation of AMP cytonemes, we expressed *htl RNAi* (*htl-i*) either under the *htl-Gal4* control or in clones under *htl>FRT>Gal4* control (Fig. 5H-M). In control experiments, Lifeact:GFP-marked WT AMPs/AMP clones extended orthogonal cytonemes when localized in the disc-proximal location and lateral cytonemes when present in the disc-distal location. In contrast, *htl* knockdown AMPs exclusively lacked the orthogonally polarized disc-specific cytonemes (Fig. 5H-J, Table 2). Importantly, the lateral polarity of AMPs/AMP cytonemes were unaffected by the *htl-i* condition. Thus, activation of Htl signaling in AMP is required specifically for their disc-specific orthogonal polarity.

Cytoneme-mediated Htl signaling controls asymmetric AMP fates and positioning.

Since Htl signaling is required for the disc-specific polarity of AMP cytonemes, the effects of the loss of Htl signaling on AMPs are expected to be similar to cytoneme-deficient *dia-i* expressing AMPs. Indeed, *htl* knockdown in Lifeact:GFP and nls:GFP-marked AMPs showed fewer AMPs and AMP layers with a concomitant increase in the homotypic AMP-AMP adhesion, mimicking fusogenic responses (Fig. 5H-H"; K-K"; Tables 1,2). Importantly, unlike *dia-i*-expressing AMPs that completely had lost polarity, *htl-i* expressing AMPs lost polarity exclusively toward the disc. The mutant nls:GFP-marked AMPs, did not orient toward the disc and aligned parallel to the disc plane, despite their proximity to the disc (Fig. 5K-L).

Moreover, when we generated *htl-i* expressing AMP clones (marked either with Lifeact:GFP or nls:GFP), all of the mutant clones were positioned exclusively in the disc-distal layer and only had laterally oriented cytonemes (Fig. 5I-M'). Phospho-histone (PH3)-staining (anaphase marker) in tissues harboring randomly distributed nls:GFP-marked WT and *htl-i*-expressing clones showed that mitotically active AMPs occupy only the disc-proximal niche, as reported before [30], and the presence of *htl-i* mutant clones in wing disc did not affect the normal organization and activity of the neighboring AMPs in the same tissue. Thus, cytoneme-meditated Htl signaling is required for the disc-specific AMP polarity, positioning, and fates.

Altogether, these results showed that AMP cytonemes are required for two interdependent functions - selective adherence to disc cells and asymmetric Htl signaling. Integration of these two functions through cytonemes constitutes a self-regulatory loop, where polarized cytonemes are essential for niche adhesion and Htl signaling, and Htl signaling, in turn, is essential for the disc-specific cytoneme polarity and adhesion. Consequently, FGF signaling and AMP adhesion promote each other in a coordinated interdependent manner. However, to create and maintain asymmetrical patterns of these functions among disc-associated AMPs, we suggest that the Htl ligands must be presented and dispersed from wing disc cells in a restricted target-specific manner through cytonemes.

Spatially restricted expression of two FGFs controls asymmetric signaling and AMP organization.

Htl is known to bind to two FGF-ligands, Pyramus (Pyr) and Thisbe (Ths) [46]. Ths is expressed in the wing disc notum [35] and is a likely candidate to control the overlaying AMPs (Fig. 6A). However, Htl-expressing AMPs and AMP cytonemes also populate the disc hinge area that lacks *ths* expression (Movie S8). Although Pyr expression in the disc has not been reported, we predicted that Pyr might be expressed in the hinge area to support the AMPs that lie over the hinge. Therefore, to identify *pyr* expression in the wing disc, we first generated a *pyr-Gal4* fly using CRISPR/Cas9-based genome editing and verified its accurate spatial expression as described in Methods (Figs. 6B; S3A-E). Indeed, in the wing disc, *pyr-Gal4* was highly expressed in the disc hinge areas that lacked *ths* expression (Fig. 6C). When both AMPs and the *pyr* source were marked, the spatial distribution of AMPs over the hinge precisely coincided with the *pyr* expressing zone. Thus, the wing disc niche is subdivided into two FGF-producing niches: the Pyr-expressing hinge and the Ths-expressing notum.

Since Pyr and Ths signal through the same Htl receptor [46], different FGF-expressing sources might locally support different muscle-specific AMPs in distinct compartments. Interestingly, the disc hinge area is known to harbor direct flight muscle (DFM)

progenitors, which express a homeobox transcription factor, Cut, while the indirect flight muscle (IFM) progenitors, which express high levels of Vestigial (Vg) and low levels of Cut, occupy the notum [33]. Cut and Vg immunostaining of discs with CD8:GFP-marked *pyr* and *ths* sources revealed that the *pyr*-expressing and *ths*-expressing zones spatially correlated with the DFM and IFM progenitor distribution, respectively (Fig. 6G-I). Although we did not explore the direct role of FGF signaling in Cut or Vg expression in AMPs, the above results suggest that the Pyr-expressing and Ths-expressing niches promote the occupancy of different muscle-specific AMPs within the respective FGF-expressing zones. Since, Htl is a common receptor for both FGFs, it is possible that cytoneme-mediated adherence and contact-dependent signaling coordinate ligand-specific asymmetric signaling and organization of AMPs.

To test this model, we performed *RNAi*-mediated knockdown of *ths* (*ths-i*) and *pyr* (*pyr-i*) from their respective sources and visualized niche-specific effects while marking the resident AMPs with CD2:GFP (Fig. 6J-P''). In comparison to the control, *ths-i* expression under *ths-Gal4* led to fewer AMPs and AMP layers exclusively over the *ths* zone (Fig. 6J-L). The remaining AMPs over the *ths*-expression zone had reduced dpERK and fewer disc-specific polarized cytonemes (Fig. 6K',L'). However, *ths-i* conditions did not produce any detectable defects in dpERK signaling and AMP cytonemes over the *pyr*-expressing hinge (Fig. 6M-M''). Similarly, *pyr>pyr-i* conditions had fewer AMPs, AMP cytonemes, and, consequently, less dpERK signaling over the *pyr-Gal4*-expressing hinge area (Fig. 6N-O''). However, it did not affect signaling and polarized cytonemes in AMPs over the *ths* zone (Fig. 6P,P'). These results showed that disc-derived Pyr and Ths are required to promote signaling and cytoneme formation exclusively in their respective zones.

Cytoneme-mediated Pyr and Ths distribution drive ligand-specific asymmetric AMP organization.

To examine if Pyr and Ths are exchanged with the niche-adhering AMPs in a restricted manner via cytonemes, we generated Ths:GFP and Pyr:GFP constructs and expressed them under *ths-Gal4* and *pyr-Gal4*, respectively (Fig. 7A-I'', see Methods). Despite

overexpression, Pyr:GFP and Ths:GFP were distributed exclusively in the AMPs that adhered to their own expression zones (Fig. 7A-D'). We also detected a significant increase in the numbers of AMPs and AMP layers exclusively within the niche that overexpressed the signals (Fig. 7E-F'; Table S4).

High-resolution imaging of tissues expressing GFP-tagged FGFs from their own sources and harboring mCherryCAAX-marked AMPs revealed that disc-adhering AMP cytonemes localized either Ths:GFP or Pyr:GFP puncta depending on the signal source they contacted (Fig. 7G-I"). Notably, Ths:GFP-expressing wing disc cells localized high levels of the signal at their apical junctions, where AMP cytonemes had established contacts (Fig. 7H,H'). This suggested a mechanism of polarized signal presentation and exchange. Similarly, Pyr:GFP appeared to be limited subcellular organelle, which might limit its release. These results are consistent with cytoneme-mediated target-specific Pyr and Ths exchange resulting in polarized niche-AMP signaling.

To examine if an ectopic Pyr and Ths expressing niche can induce cytoneme-mediated asymmetric niche organization, we ectopically expressed Pyr:GFP and Ths:GFP under *dpp-Gal4* control. Ectopic Pyr expression in the disc pouch under *dpp-Gal4* is known to induce AMP migration onto the *dpp*-expressing zone [44]. To detect the AMP-niche relationship, we marked the *dpp* source with mCherryCAAX and probed AMPs by Cut immunostaining. As expected, Ths:GFP and Pyr:GFP expression from the *dpp* source established ectopic niches, with AMPs orthogonally organized into a multi-stratified layer (Figs. 8A-F; S3F-H). Despite overexpression, Ths:GFP and Pyr:GFP puncta were asymmetrically distributed only to the disc-proximal AMPs (Fig. 8C-F).

Moreover, Cut (DFM-specific) and Vg (IFM-specific) staining revealed that the proximal position of the Pyr:GFP-expressing niche was selectively adhered by Cut-expressing AMPs and Vg-expressing AMPs were sorted out into the disc-distal location (Fig. 8C,D). Similarly, Vg-expressing AMPs selectively adhered to the Ths:GFP-expressing niche and high Cut-expressing AMPs were sorted to the distal layers (Fig. 8E,F). Thus, Pyr

and Ths expressed from the *dpp* source also asymmetrically organized signaling and ligand-specific cellular patterns.

To further visualize orthogonally polarized cytonemes from the niche-adhering AMPs, we imaged mCherryCAAX-marked AMPs that occupied the ectopic Ths:GFP-expressing *dpp* source. Proximal AMPs were polarized toward the niche and extended niche-invading cytonemes (Fig. 8G). Single optical YZ sections across these cytonemes showed Ths:GFP enrichment along the cytoneme shafts, suggesting cytoneme-mediated Ths:GFP uptake from the localized source (Figs. 8G'-G'''; S3I-I'). These results showed that the localized expression and cytoneme-mediated target-specific signaling establish asymmetric signaling and AMP organization in the niche.

DISCUSSION

These findings show that cytoneme-mediated target-specific signal distribution is required for generating asymmetric signaling and AMP organization within the wing disc niche. These results also uncovered a mechanism by which cytoneme-mediated polarized signaling can generate and sustain asymmetric patterns in the stem cell niche (Fig. 8H).

Previously, well-characterized *Drosophila* stem cell niches have revealed that the niches require two basic strategies to function - adhesive interactions between niche and stem cells and asymmetric signaling [47]. In this study, with high-resolution imaging in combination with genetic analyses, we found that AMPs employ cytonemes to integrate these two essential functions, thereby constituting a central self-regulatory pathway, which can generate and maintain diverse niche-specific asymmetric signaling and cellular organization.

We found that the central pathway is constituted of three essential and interdependent events: First, AMPs extend cytonemes that orient toward the wing disc niche and invade through the intercellular space of niche epithelial cells to

adhere the AMPs to the disc cell junctions. This is a dynamic process and multiple AMPs share the limited wing disc space through cytonemes to maintain their position. Second, these cytonemes also localize FGFR/Heartless (Htl) to select and adhere to only the FGF-producing disc areas and directly receive disc-produced FGFs through cytoneme-niche contacts. Third, and an important step, is the response of the activation of FGF signaling, which promotes AMPs to extend polarized FGFR-containing cytonemes toward the disc and reinforce their adherence to the selected signal-producing niche (Fig. 8H). Thus, without the disc-specific polarity and adhesion of cytonemes, AMPs are unable to activate FGF signaling, and without FGF signaling, AMPs are unable to extend cytonemes toward the disc to adhere to the niche.

Our results suggest that this interdependent relationship of the cause and consequence of cytoneme-mediated interactions ensures a well-coordinated integration of multiple functions, including sensing and adhering to a specific FGF-producing niche, receiving FGFs from the niche, and responding to the same niche-derived FGF to determine AMP position and fates. Our results also revealed how this pathway could lead to diverse asymmetric patterns of FGF signaling and AMP organizations (Fig. 8H).

For instance, it was known that the polarized asymmetric divisions of the disc-proximal AMPs lead to the formation of a multi-stratified layer orthogonal to the disc [30]. However, the basis of this polarity was unclear. Our results suggest that the presence or absence of cytoneme-mediated contacts can provide a way to determine the polarity, position, and fates of AMPs in relation to the FGF-producing wing disc niche. Disc-proximal AMPs can determine their disc-specific positions and polarity by selectively orienting their cytonemes toward the FGF-producing niche, and receiving FGF by adhering to the niche. The activation of FGF signaling, in return, reinforces and maintains the niche adhering polarity, affinity, and positional identity in proximal AMPs. With increased orthogonal distances from the disc, distal AMPs lose niche adhesion, polarity, and FGF signaling, which in return, primes these AMPs to migrate

away from the disc and acquire various morphologic features required for fusion and differentiation. Consequently, an asymmetric cellular and signaling pattern emerges along the p-d orthogonal axis relative to the disc in an interdependent manner.

Notably, although distal AMPs do not extend cytonemes toward the disc, they extend cytonemes toward each other and toward the TC/ASP, probably to acquire new signaling functions. For instance, AMPs are known to use cytonemes for Notch signaling with the TC/ASP [36]. Our results suggest that the TC/ASP might act as a second niche to support distal AMPs (Figs. S1C, 8H). Moreover, actin-based filopodia are also essential for AMP-myotube fusion during myogenesis [43,48]. So, filopodia/cytonemes can promote both AMP stemness and differentiation by interacting with different types of cells. We suggest that altering the contexts of cytoneme polarity and signaling contacts can alter fates, functions, and niche-specific organization of stem cells. This model is also consistent with the previous report of filopodial tethering of embryonic AMPs to surrounding muscles [49].

An example strongly supporting this model comes from the second asymmetric organization of AMPs. AMPs are known to be maintained in two distinct spatial regions of the wing disc to acquire either DFM-specific or IFM-specific fates [33]. We found that the wing disc AMP niche is subdivided into Pyr and Ths expressing zones to support DFM-specific and IFM-specific AMPs, respectively. The affinities of the DFM precursors for the Pyr zone and IFM precursors for the Ths zone are evident from the ectopic induction of Pyr and Ths expressing niches (Fig. 8C-F). Although Pyr and Ths signal through the same receptor, our results suggest that their cytoneme-mediated contact-dependent signaling inputs allow differential ligand-specific self-organization of DFMs and IFMs within distinct FGF-expressing niches.

Our results indicate that to control the asymmetric patterning of AMPs, the wing disc restricts random secretion/dispersion of FGFs and targets their release only through cytoneme-mediated AMP-niche contacts. A significant previous discovery suggests that Pyr is a transmembrane protein and transmembrane tether controls its spatiotemporal

functions [50]. Moreover, Pyr is apically enriched within the source cell [50]. We predict that the membrane tethering is critical to control cytoneme-mediated Pyr signaling, similar to what was observed for a GPI-anchored FGF, Branchless that controls *Drosophila* ASP development [21]. Similarly, apical enrichment of Ths:GFP suggests a spatial asymmetry in the Ths release. Thus, the core self-regulatory loop of cytoneme-mediated signaling in recipient cells can essentially self-organize and reinforce any shapes and spatial patterns, but its final architecture is dependent on the context-specific asymmetry in contact-dependent presentation and reception of extrinsic signaling cues.

FGF signaling has been implicated for a wide range of functions, including self-renewal and differentiation of diverse vertebrate stem cells, including hematopoietic, neural, spermatogonial, prostate, and bone marrow-derived mesenchymal stem cells [51,52]. Htl signaling was also implicated in controlling AMP proliferation [35,44]. However, our results establish a unique perspective, in which the same FGF signaling can determine and balance between a range of functions, including positional identity, self-renewal, differentiation, proliferation, and polarity/organization, simply by modulating when and where AMPs establish cytoneme-mediated contacts within a dynamic microenvironment (Fig. 8H). It also explains how two FGFs that act through the same receptor, Htl can produce different signaling outcomes.

Asymmetric signaling microenvironment is required not only to hold stem cells, control their proliferation, and repress differentiation inside the niche, but also to guide organized patterns of differentiation of stem cells outside the nice [47]. Therefore, our findings, showing how polarized signaling and cellular interactions through cytonemes generate and maintain diverse niche-specific signaling and cellular asymmetry, have broad implications.

Acknowledgments

We thank Drs. T.B. Kornberg, G. M. Rubin, K. A. Guss, and S. Roth for sharing reagents; Drs. N. Andrews (U. Maryland), L. Du (U. Maryland), and T. Kornberg (UCSF) for comments on the manuscript; Drs. T.B. Kornberg and G. O. Barbosa (UCSF) for sharing the design of the culture chamber for live imaging. A.P. acknowledges a fellowship from UMD CMNS Dean's Matching Award for T32 GM080201; This work was funded by NIH R35GM124878 and R35GM124878-03S1 grants to SR and intramural funding from NIBIB-NIH to H.S.

The authors declare no competing financial interests.

Author Contributions

S.R. supervised the work and designed the project; H.S. supervised Multiview microscopy; T.M. supervised TEM; A.P. conducted all experiments, and Y.W., X.H., and Y.S. conducted experiments with Multiview microscopy; S.R., A.P., H.S., Y.W., T.M. contributed to writing the paper.

FIGURES AND LEGENDS

Figure 1

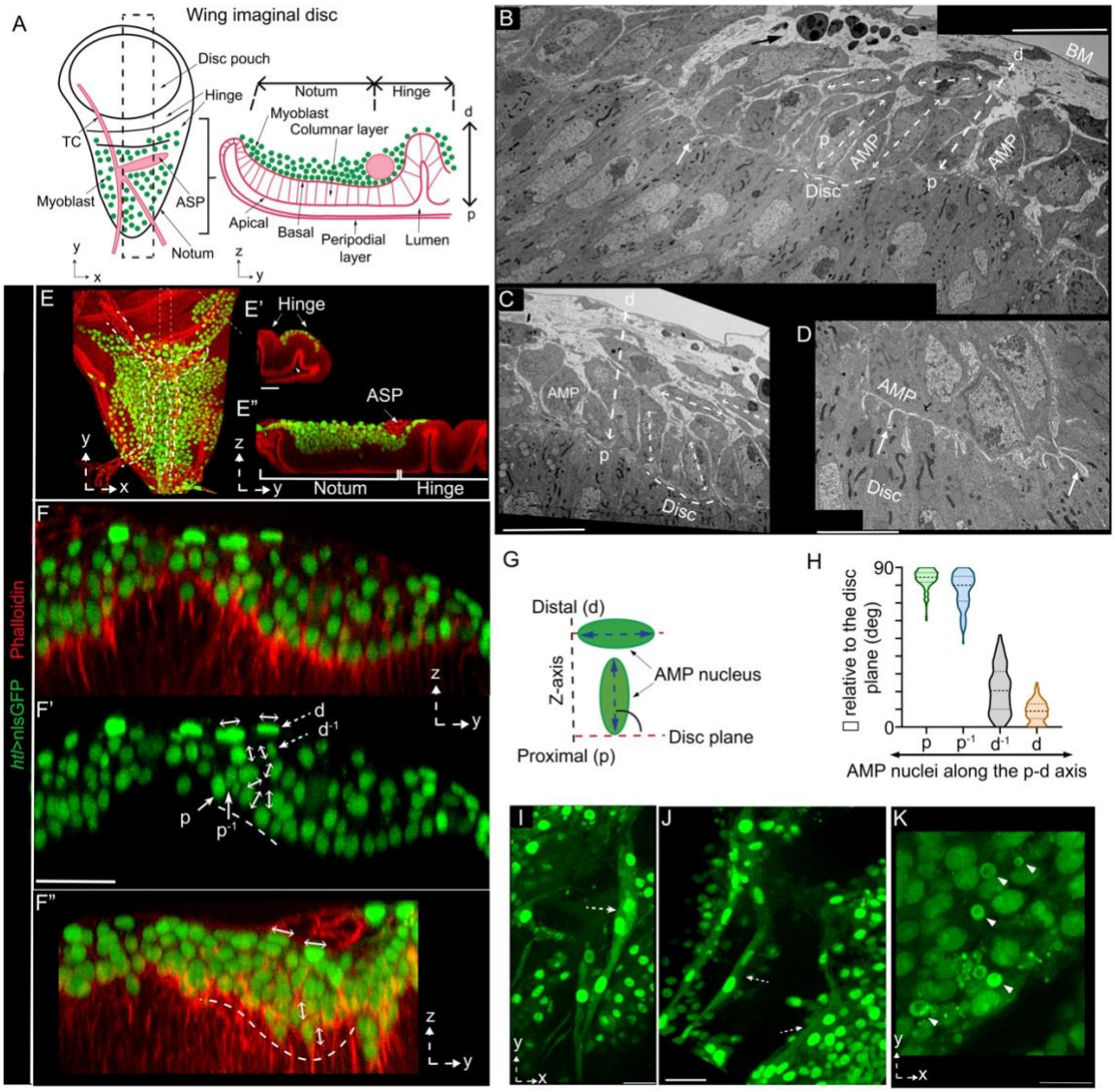

Figure 1: Correlation of the AMP position and polarity relative to the disc. (A) Drawing of an L3 wing disc showing the spatial organization of AMPs, wing disc notum and hinge areas, and ASP and TC; dashed box (left), ROI used for all subsequent YZ cross-sectional images. **(B-D)** TEM sections (*w*^{1118}) showing YZ views of different disc areas, showing changes in AMP polarity along the proximo (p)-distal (d) axis, orthogonal to the disc (B,C), and cytoneme-like projections (white arrow) from the disc-proximal AMPs (D; see Fig. S1A,A'); double-sided arrows, long axes of elliptical AMPs; black arrow, non-polar cells in distal layer. **(E-E")** Spatial organization of nls:GFP-marked AMP nuclei, orthogonal to the wing disc notum (E,E") and hinge (E,E') as illustrated in A. **(F-H)** Cross-sections (as indicated in F-F") of wing disc regions harboring nls:GFP-marked AMPs, showing altered nuclear orientation (double-sided arrows) along the p-d axis, relative to the distance from the disc plane (red, phalloidin; dashed line); F', green channel of F; dashed and solid arrows, distal and proximal layer cells, respectively; G,H, graph (H) showing quantitative analyses of nuclear orientation (angles (θ) between AMP nuclei and the disc planes as shown G) in the different locations: p - proximal, d - distal, p^{-1} - one layer above p; d^{-1} - one layer below d. **(I-K)** Single XY optical sections of the discs, showing diverse morphologies of distal AMPs; dashed arrows, elongated syncytial cells; arrowhead, small nonpolar cells (also see Fig. S1B-D'). **(E-F")** red, phalloidin, marking tissue outlines (also indicated by dashed line). Genotypes: see methods. Scale bars: 20μm; (B,C,K): 10μm; (D): 5μm.

Figure 2

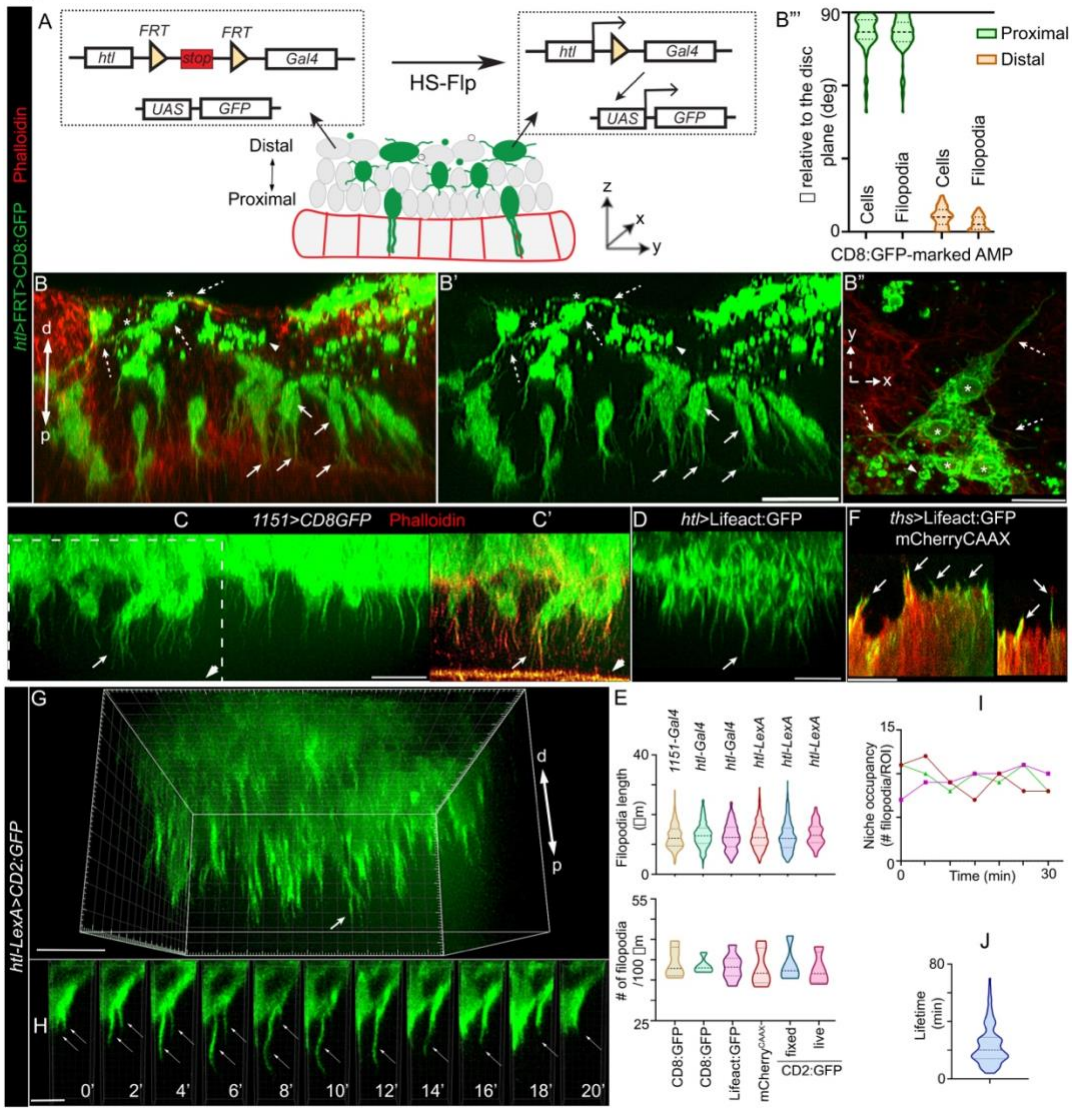

Figure 2: Disc-specific AMP polarity and adhesion are linked to the polarized AMP cytonemes. (A) Schematic depiction of *htl>FRT>stop>FRT>Gal4* construct and its application in inducing FLIP-out clones exclusively in AMPs (also seeS1E,F). **(B-B")** Images of a wing disc harboring random CD8:GFP-marked AMP clones showing the orthogonal and lateral polarity of cells and their cytonemes, relative to the disc plane; arrow and dashed arrow, proximal and distal AMPs, respectively; arrowhead, distal small non-polar cells; * adherent distal AMPs; phalloidin (red), actin-rich disc-AMP junction and cell cortex; (also see Fig. S1;G-H"); B', GFP channel of B; B"', Violin plots showing angles (θ) between proximal and distal AMPs and their cytonemes relative to their underlying disc plane (see Fig.1G). **(C-E)** Comparison of AMP cytonemes (arrows) marked by various fluorescent proteins driven by different transcription drivers, in fixed and live tissues, as indicated; arrowhead, actin-rich (phalloidin-marked) apical junction of disc epithelium; E, Graphs comparing length and numbers (count/100 μm length of AMP-disc interface) of orthogonal cytonemes (arrow). **(F)** Actin-rich cytonemes (arrow) from wing discs marked by mCherryCAAX and Lifeact:GFP (fixed). **(G-J)** Live dynamics of AMP cytonemes; G, 3D-rendered image from p-to-d direction; H, dynamics of few cytonemes (arrow) that shared the same niche space (every 2' frames shown, also see Movie S1-S4); I, Graphs showing numbers of niche-occupying cytonemes over time within selected ROIs; three graph colors, three discs; J, Graph showing the distribution of cytonemes lifetimes (see Table S3). Genotypes: see methods. Scale bars: 20μm; (H): 5μm.

Figure 3

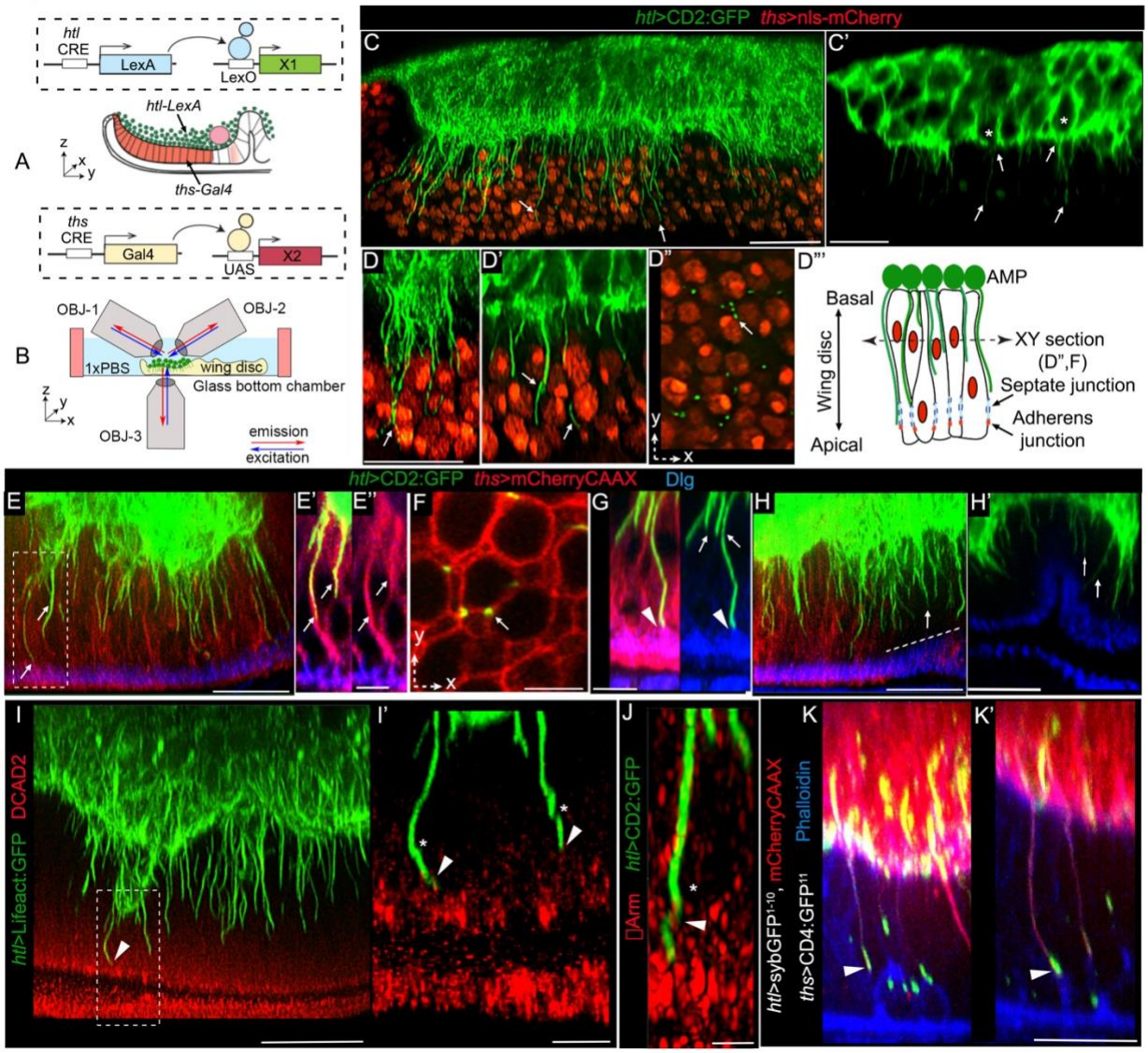

Figure 3: AMP cytonemes anchor AMPs to the wing disc adherens junctions. (A-B) Schematic depictions of the genetic strategy (A) used to simultaneously mark AMPs and the disc notum, and imaging strategy (B) using multi-view microscopy for deep-tissue imaging. **(C-D''')** Triple-view confocal imaging showing CD2:GFP-marked orthogonal cytonemes (arrow) from the orthogonally polarized proximal AMPs (*, in C') and their distribution through the intercellular space between nls:mCherry-marked disc cells (C,D, D'); D'', D''', A single XY cross-section of disc, as illustrated in D''', showing multiple cytonemes sharing the same intercellular space. **(E-H')** CD2:GFP-marked AMP cytonemes at the intercellular space of mCherryCAAX-marked wing discs approaching apical adherens junctions (Dlg stain, blue); E',E'', dashed box area in E; F, XY cross-section of disc showing niche sharing by multiple cytonemes; G, Airyscan image of cytoneme tip approaching adherens junction (arrowhead), H,H', AMP cytonemes niche in both *ths-Gal4* expressing and non-expressing areas. **(I-J)** Tip regions of AMP cytonemes contacting disc adherence junction that is marked with DCAD2 (I-I') and Arm (J); *, helical twists in cytonemes; arrowhead, contact sites; I', zoomed-in image from ROI in I. **(K-K')** Synaptic cytoneme-disc contacts mapped by syb-GRASP (see Methods) between the mCherryCAAX-marked (also expressing sybGFP$^{1-10}$) cytonemes and the actin-rich (phalloidin-stained, blue) apical junction of CD4:GFP^{11}-expressing wing-disc epithelium. All images are YZ cross sections unless noted. Genotypes: see Methods. Scale bars: 20μm; (E,E',I',F,G): 5μm; (J) 2μm.

Figure 4

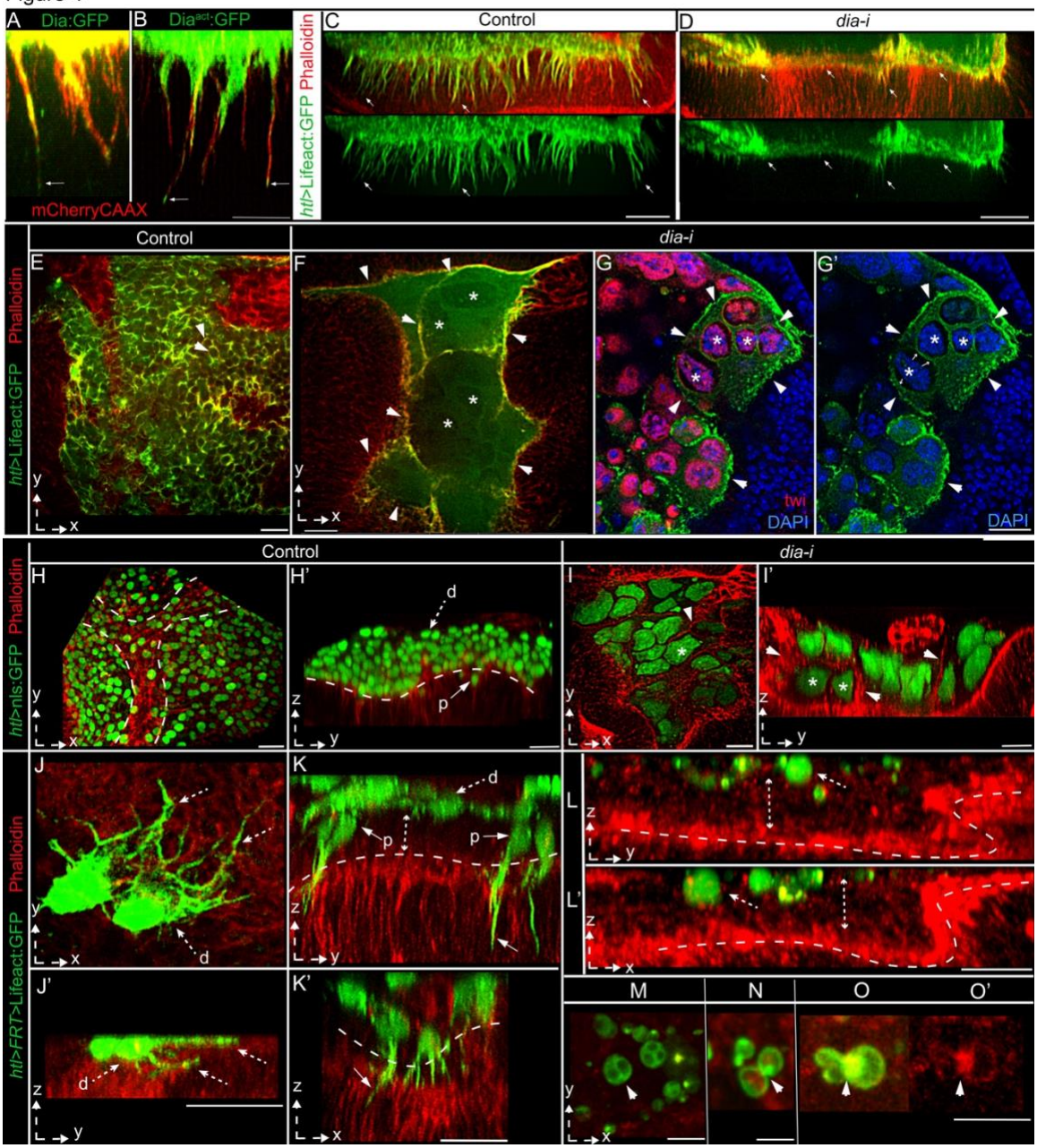

Figure 4: Disc-cytoneme adhesion determines AMP position and fates. (A-D) AMP cytoneme formation depends on Dia; A,B, mCherryCAAX-marked AMP cytonemes localizing Dia:GFP (A) and Dia^{act}:GFP (B); C,D, Loss of cytonemes (arrow) in Lifeact:GFP-marked AMPs expressing *dia-i* (D); C, control for D. **(E-I')** Comparison of control disc (E,H,H') and disc expressing *dia-i* in AMPs under *htl-Gal4*, showing changes in the number of AMPs and AMP nuclei, morphologies, and orientations relative to the disc; G,G', DAPI and Twi-stained; E-G' and H-I', AMPs expressing Lifeact:GFP and nls:GFP, respectively; red, phalloidin; arrowhead, actin-rich cell outline; *, examples of giant nuclei within a large chamber; arrows in G' show the cytoplasmic space and thin Lifeact:GFP-marked membrane cortex surrounding each giant nucleus; dashed line in H and H', tracheal outline and AMP-disc junction, respectively. **(J-O)** Comparison between control (J-K') and *dia-i*-expressing (K-O') AMP clones for their proximo-distal localization, polarity, and morphology; dashed arrow, distal cell/cytonemes, solid arrow, proximal cell/cytonemes, dashed line, AMP-disc junction, dashed double-sided arrow, space between basal disc surfaces and distal clones; M-O', arrowhead, multi-nucleated cells (M), actin-rich (phalloidin stained and Lifeact:GFP-marked) fusogenic synapse (N-O'). XY or YZ views are indicated. Genotypes: see methods. Scale bars: 20μm; (A,B,M-O): 10μm.

Figure 5

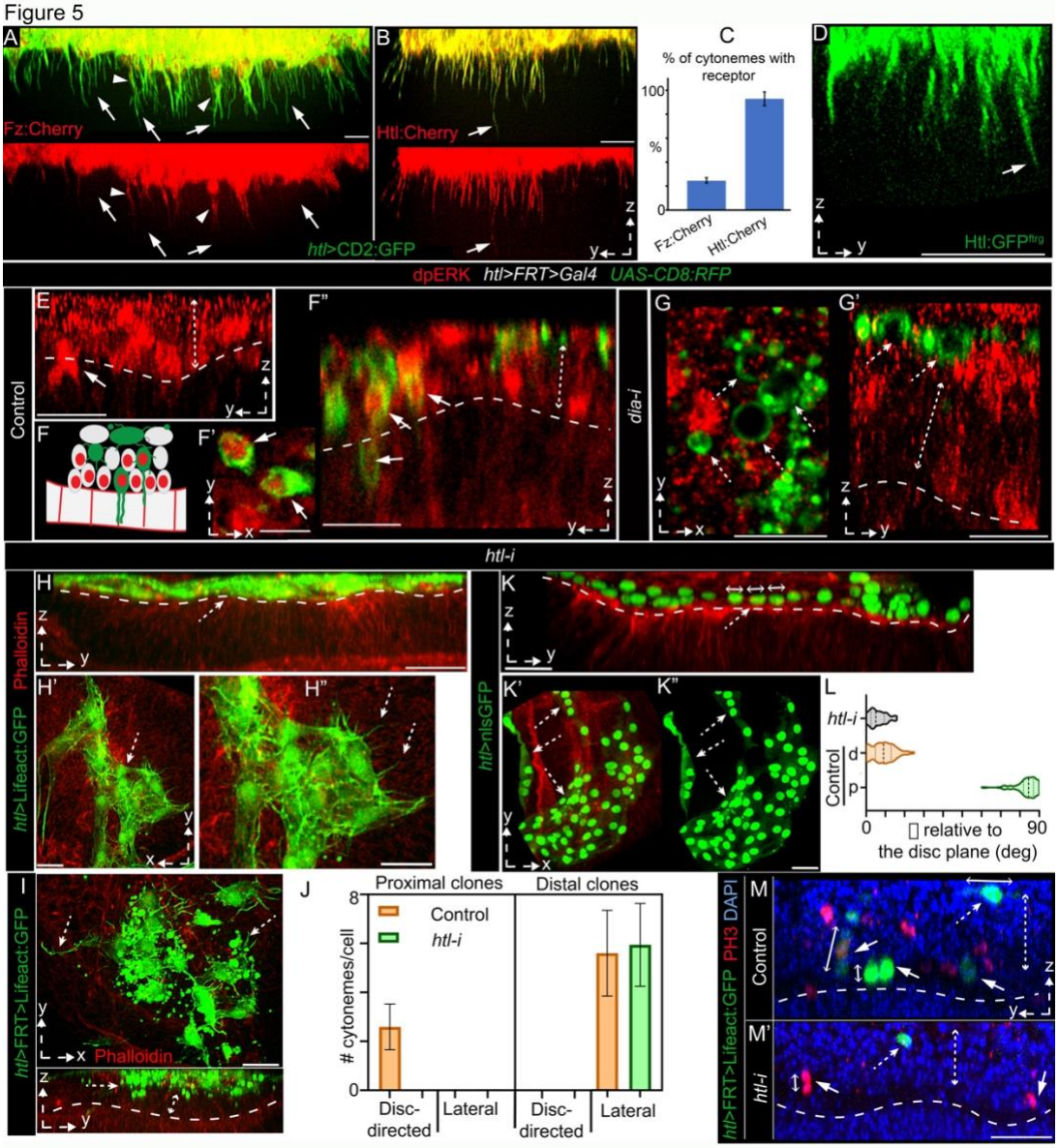

Figure 5: Disc-adhering AMP cytonemes localize Htl for niche occupancy and FGF signaling. (A-C) CD2:GFP-marked AMP cytonemes, localizing Fz:mCherry (A) and Htl:mCherry (B); arrowhead, cytoneme base; arrow, cytoneme tip; C, graph showing the percent of orthogonal cytonemes localizing Fz:mCherry (498 cytonemes, 8 discs) and Htl:mCherry (119 cytonemes, 5 discs; $p<0.0001$). **(D)** Htl:GFP^{fTRG} localization on orthogonal AMP cytonemes. **(E-G')** CD8:RFP-marked clones (green, pseudocolored) of control and *dia-i*-expressing AMPs showing the FGF signaling state (nuclear dpERK, red); E, control discs without clone induction; F, drawing depicting F''. **(H-M)** Effects of *htl-i* expression under either *htl-Gal4* (H-H'', K-L) or *htl>FRT>Gal4* (single cell clones; I,J,M,M'); **(H-H"** and **K-L)** Discs harboring either Lifeact:GFP-marked (H-H'') or nls:GFP-marked (K-L) *htl-i* expressing AMPs showing selective loss of orthogonal cytonemes (H-H"), cell polarity (K,L), reduced AMP number and layers (H,K), and fusogenic responses (H',I,K',K''); L, graphs comparing AMP nuclear angles (θ) in control (n=5 discs, 125 proximal cells, 58 distal cells) and *htl-i*-expressing AMPs (n=3 discs, 33 cells); J, graphs comparing orthogonal and lateral cytoneme numbers per Lifeact:GFP-marked AMP clones as indicated; **(M,M')** Discs with DAPI and PH3 staining showing relative location and orientation of nls:GFP-marked control (M) and *htl-i*-expressing (M') AMP clones. **(E-M)** dashed arrow, distal cells/cytonemes; solid arrow, proximal cell/cytonemes; dashed line, AMP-disc junction; dashed double-sided arrow, space between the basal disc surface and the distal layer. Genotypes: see Methods. Scale bars: 20μm; (F'): 10μm.

Figure 6

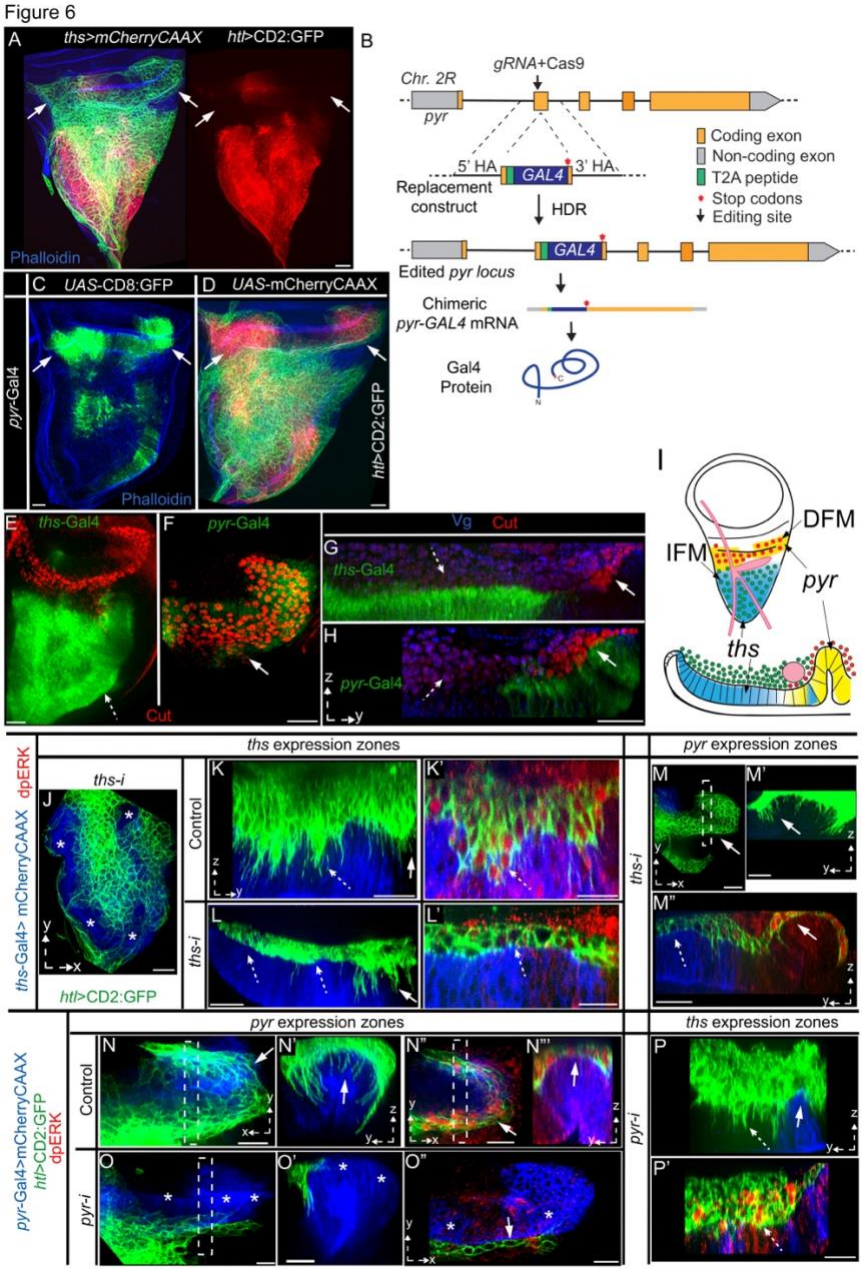

Figure 6: Wing discs express Pyr and Ths in distinct zones to create two distinct AMP niches. (A) Spatial patterns of *ths-Gal4*-driven mCherryCAAX expression in the wing disc notum and the distribution of CD2:GFP-marked AMPs; arrow, *ths* expression-free hinge area; right panel, red channel from the left panel. **(B)** Scheme depicting the genome editing strategy to generate a *pyr-Gal4* enhancer trap construct (also see Fig S3E-I). **(C,D)** Wing disc expression patterns of *pyr-Gal4*-driven CD8:GFP (C) and mCherryCAAX (D) and its spatial correlation to the AMP distribution (D, arrow). **(E-I)** Images showing CD8:GFP-marked *ths-Gal4* and *pyr-Gal4* expression zones in wing discs and their correlation with the localization of IFM-specific (high Vg, blue; low Cut, red; arrow) and DFM-specific (high Cut, red; dashed arrow) progenitors; I, schematic depicting the results of E-H. **(J-M")** Images, showing effects of *ths-i* expression from *ths* source (*ths-Gal4*; mCherryCAAX-marked, blue) on the resident AMPs (AMP number, cytonemes, polarity, multi-layered organization, and dpERK signaling (red)) and non-resident AMPs (over the unmarked *pyr*-zone). **(N-P')** Images showing effects of *pyr-i* expression from *pyr* source (*pyr-Gal4*, blue area) on the resident AMPs and non-resident AMPs (unmarked *ths*-expression zone). **(J-P')** solid arrows, *pyr* expression zone; dashed arrow, *ths*-expression zone; dashed box, ROIs used to produce YZ views. Genotypes: see methods. Scale bars: 20μm.

Figure 7

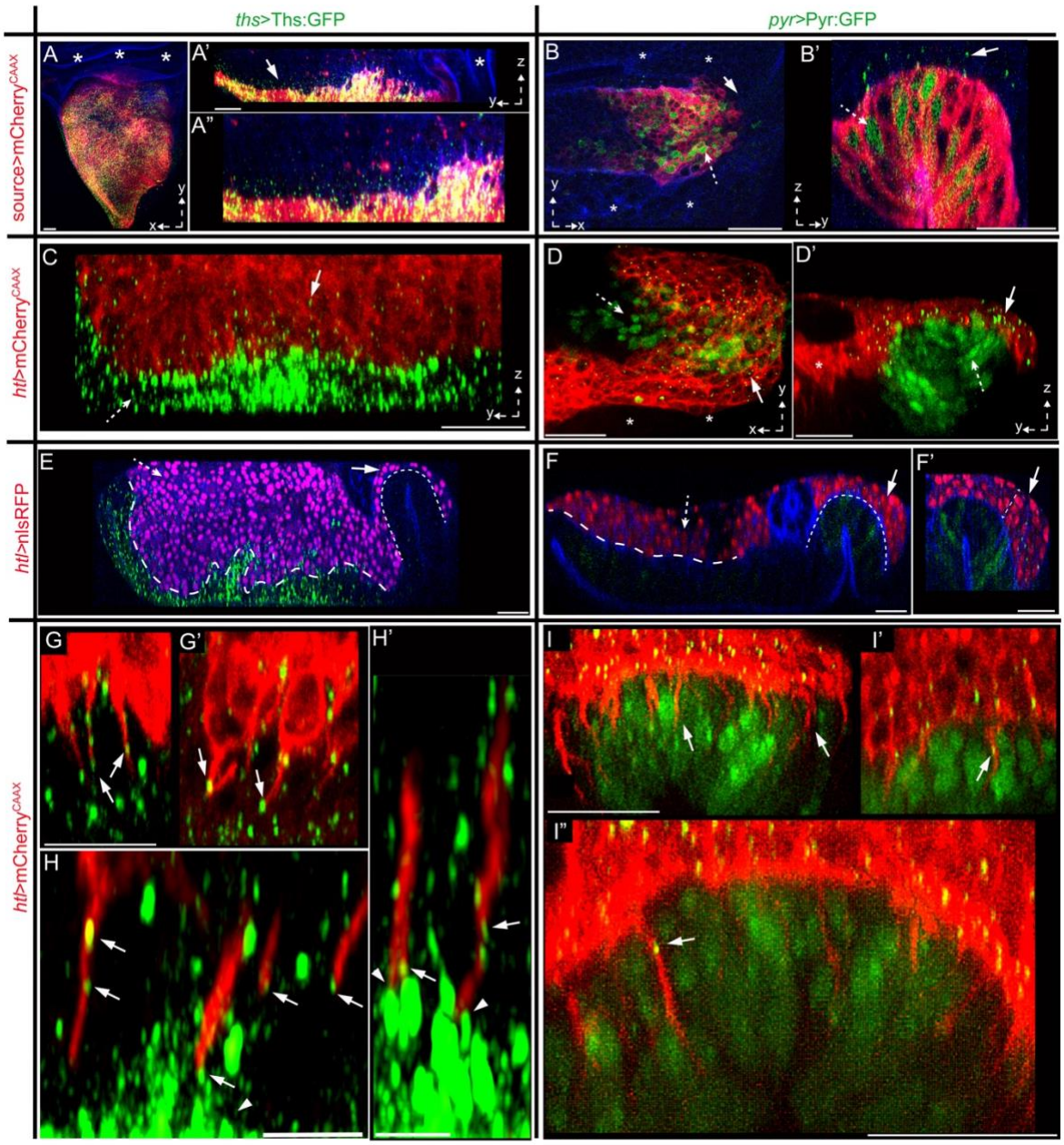

Figure 7: Cytoneme-mediated FGF exchange generates niche-specific asymmetric signaling. (A-B') XY and YZ views (as indicated) of wing discs expressing either Ths:GFP (A-A") or Pyr:GFP (B-B') under *ths-Gal4* or *pyr-Gal4*, source marked with mCherryCAAX. **(C-D')** Images of wing discs harboring mCherryCAAX-marked AMPs; wing discs expressing either Ths:GFP or Pyr:GFP as indicated. **(A-D')** dashed arrow, signal in the source; arrow, non-autonomous punctate distribution in the AMP; *, non-expressing areas of the lacking signal distribution. **(E-F')** Wing discs expressing either Ths:GFP or Pyr:GFP as indicated, showing niche-specific effects of signal overexpression on proliferation of niche-resident and non-resident AMPs (nls:GFP marked); thick and thin dashed line, interface between AMPs and *ths*- and *pyr*-expression zones, respectively; dashed and solid arrows, effects on *ths*- and *pyr*-expression zones, respectively; double-sided dashed arrow (F'), increase in the AMP layer thickness. **(G-I")** YZ views of wing discs expressing either Ths:GFP or Pyr:GFP as indicated and harboring mCherryCAAX-marked AMPs, showing disc-invading cytonemes receiving GFP-tagged signal (arrow) from the disc cells; arrowheads, apical enrichment of signal. Genotypes: see Methods. Scale bars: 20μm; H-H', 5μm.

Figure 8

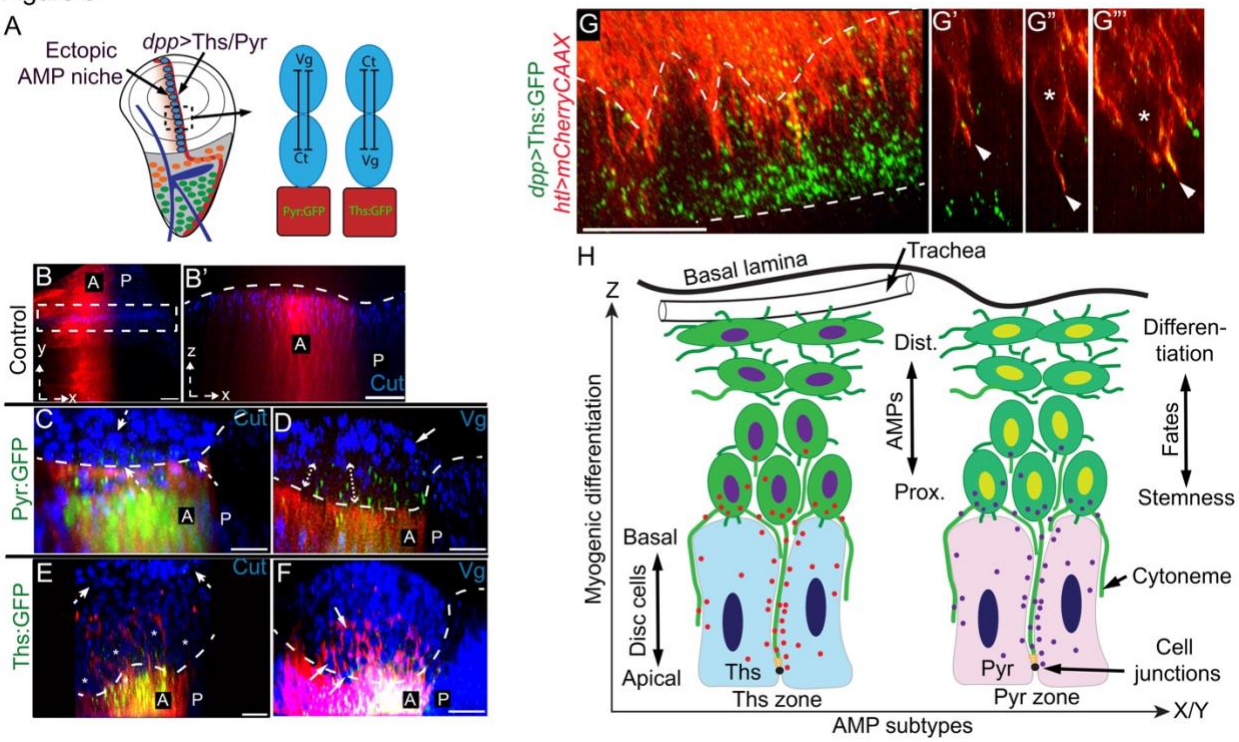

Figure 8: Cytoneme-mediated ligand-specific asymmetric signaling and organization in ectopic niches. (A-F) Asymmetric FGF signaling and ligand-specific organization of different muscle-specific AMPs (blue, stained either with αCut or αVg) in ectopic niches expressing either Pyr:GFP or Ths:GFP, as indicated, under *dpp-Gal4* (mCherryCAAX-marked area); A, Drawing depicting the experiments and results in B-F; dashed line, AMP-disc junctions; B', XZ section from ROI in B; dashed and solid arrows, Ct and Vg expressing AMPs, respectively; double-sided arrow (D), proximal zone of Pyr:GFP expressing niche lacking Vg-positive AMPs. **(G-G'''')** Wing disc pouch expressing Ths:GFP under *dpp-Gal4* and showing mCherryCAAX-marked AMP and AMP cytonemes; *, proximal AMPs with orthogonal polarity and cytonemes; G''-G''', single optical sections showing Ths:GFP on cytonemes (arrowheads); dashed lines, disc epithelium. **(H)** Model for the niche-specific asymmetric signaling and organization by cytonemes. Genotypes: see Methods. Scale bars: 20μm.

METHODS

Drosophila melanogaster stocks

All flies were raised at 25 °C with 12 h/12 h light/dark cycle unless noted. This study: *htl-LexA*, *pyr-Gal4/CyO*, *htl>FRT>stop>FRT>Gal4*, *UAS-Pyr:GFP*, *UAS-Ths:GFP* and *LexO-Htl:mCherry*. All new transgenic injections were performed by Rainbow Transgenic Flies, Inc. Bloomington Drosophila Stock Center: *UAS-CD8:GFP*, *UAS-CD8:RFP*, *UAS-mCherryCAAX*, *LexO-CD2:GFP*, *UAS-Eb1:GFP, UAS-Lifeact:GFP*, *UAS-nls:GFP*, *UAS-nls:mCherry*, *htl-Gal4*, *ths-Gal4/CyO*, *UAS-Dia:GFP*, *UAS-ΔDAD-Dia:GFP*, *UAS-pyrRNAi*, *UAS-diaRNAi, hs-Flp*, *{nos-Cas9}ZH-2A* and w^{1118}. Vienna Drosophila Resource Center: *htl:GFP*^{fTRG}, *UAS-htlRNAi,* and *UAS-thsRNAi*. Other sources: *LexO-nsyb:GFP*$^{1-10}$, *UAS-CD4:GFP*^{11} [20]. *LexO-mCherryCAAX* [15]. *dpp-Gal4/CyO*, *LexO-Fz:mCherry* and *1151-Gal4* [36].

Molecular cloning and generation of transgenic *Drosophila* lines

All overexpression constructs described were cloned using the primers and cloning kits listed in the Key Resources Table following manufacturers' protocols. In *UAS-Pyr:GFP*, an ectopic super-folder-GFP sequence was inserted in frame between T_{208} and T_{209} of the original 766 amino-acid-long Pyr. In *UAS-Ths:GFP*, the 'VEGQGG linker- super-folder-GFP- GSGGGS linker' sequence was inserted in frame between S_{137} and V_{138} of the original 748 amino acids long Ths. *LexO-Htl:mCherry* consists of a *htl* CDS amplified from genomic DNA fused in frame with a C-terminal VEGQGG-mCherry-STOP sequence in pLOT vector.

To make *pHtl-enh-FRT-stop-FRT3-FRT-FRT3-Gal4* (*htl>FRT>stop>FRT>Gal4*), *htl* cis-regulatory element from P{GMR93H07-Gal4} construct (gift from G. Rubin) was used to replace the pAct of the *pAct-FRT-stop-FRT3-FRT-FRT3-Gal4 attB* vector (Addgene #52889). To make *pBP-htl-enh-nlsLexA::p65Uw* (*htl-LexA*), the *htl* cis-regulatory element was cloned into *pBPnlsLexA::p65Uw* vector (Addgene #26230) using Gateway cloning (ThermoFisher). The resulting *htl>FRT>stop>FRT>Gal4* and *htl-LexA* constructs were injected using the phiC31 site-specific integration system into flies carrying the

attP2 landing site. For other constructs, transgenic flies were generated by P-element mediated germline transformation in w^{1118} flies.

Generation of *pyr-Gal4* transgenic *Drosophila*

To generate the *pyr-Gal4* driver, a standard method published earlier in Du et al. [57] was followed:

a) gRNA design and cloning. Single gRNA target site was selected within the second coding exon of *pyr* using the flyCRISPR Optimal Target Finder tool and was designed following methods described in Gratz et al. and Du et al. [57,58]. The gRNA selected is (PAM is underlined): gRNA: 5' ATAATATAAGTCCTGACATTGGG 3'. The genomic gRNA binding site of the host fly chosen for injection (nos-Cas9, BL# 54591) was sequence verified. *pCFD3-pyr-Gal4-gRNA* was cloned using the cloning protocol outlined in Port et al. [55].

b) Replacement cassette design. The replacement donor was designed to insert coding sequence for "T2A-nls:Gal4:VP16-STOP" expression within the second coding exon of *pyr* (Fig. S3A). Insertion of this cassette into the targeted genomic site disrupts the gRNA binding site to prevent post-editing gRNA binding. The replacement donor was produced with the 5' and 3' homology arms (HA) flanking the "T2A-nls:Gal4:VP16-STOP" cassette. The 5' HA contained 1.2kb of *pyr* genomic region upstream of the insertion site, and the 3' HA contained 1.3kb of *pyr* genomic region downstream of the insertion site. HA regions were amplified from gDNA of the nos-Cas9 fly as described in [57,59]. The T2A-nls:Gal4:VP16-STOP sequence was generated by PCR (see resource table) amplification of Gal4 template present in *pAct-FRT-stop-FRT3-FRT-FRT3-Gal4 attB* vector (Addgene). 5'HA, T2A-nls:Gal4:VP16-STOP, and 3'HA fragments were then assembled in correct 5'-to-3' order between Not1 and EcoR1 sites of the pJet1.2 vector.

The insertion of the "T2A-nls:Gal4:VP16-STOP" cassette is 25 nt after the 5' end of the exon and 21 nt before the 3' of the exon. The insertion does not affect the original splicing sites of *pyr* second coding exon or any of the *cis*-regulatory elements. This

enables the expression of a full-length *pyr* mRNA, which is tagged with the sequence of the Gal4-expressing cassette. Expression of this chimeric *pyr* mRNA in cells is probed with its translation into the nls:Gal4:VP16 protein, which can transactivate reporters under *UAS* control [57,59] (Fig.S3B-E). Translation of this chimeric mRNA begins from the WT 5' end of *pyr* mRNA, producing a 9-amino acid long N-terminal native Pyr protein, followed by the self-cleaving T2A peptide and nls:Gal4:VP16. Translation terminates at the stop codon inserted immediately after the nls:Gal4:VP16 CDS. The T2A-peptide cleaves off the 9 N-terminal Pyr amino acids from the nls:Gal4:VP16 protein. Although the chimeric mRNA contains *pyr* CDS, the presence of stop codons in all three frames immediately 3' to the nls:Gal4:VP16 CDS blocks any further downstream translation. Thus, the engineered *pyr* allele is functionally a null *pyr* allele.

c) Embryo Injection, fly genetics, and screening. *pCFD3-pyr-Gal4-gRNA* and the replacement cassette plasmids were co-injected in *{nos-Cas9}ZH-2A* (BL 54591) *e*mbryos following [57,59]. After the adults emerged, single G_0 adults were crossed to *Pin/CyO; UAS-CD8:GFP* flies. The resulting larva from each fertile cross were sorted out based on the presence of GFP expression and respective adults were individually crossed to *Pin/CyO; UAS-CD8:GFP* virgins. As soon as the F2 larvae emerged, the single F1 father from each cross was sacrificed for genomic DNA preparation and PCR-based screening as described in Du et al. [57,59]. Genomic DNA extracted from *{nos-Cas9}ZH-2A* fly served as the negative control. PCRs, screening for the presence of T2A-Gal4 within the endogenous *pyr* locus, were performed using the primers listed in the Key Resources table and illustrated in Figure S3A. PCRs using primer sets “gRNAseqF2” and “Seq2R”, and "Seq2F” and “gRNAseqR1" were used to verify T2A-Gal4 integration. PCRs using “pJet seqR” and “CseqF” were performed to check “ends-in” HDR. The correct line as determined by these PCR screens was selected for establishing final balanced fly stocks. Out of the 32 F1-parent lines selected via fluorescence screen, 30 lines underwent successful HDR. Twenty-nine lines were determined to be “ends-out” while one line was determined to be “ends-in”. Two “ends-out” fly lines were used to prepare high-quality genomic DNA for full sequencing of the engineered locus. These flies were outcrossed to establish final stocks for subsequent

use. The accurate *pyr-Gal4* expression patterns in flies were confirmed by comparing the observed patterns with the published *pyr* mRNA in-situ hybridization patterns [60,61] (Fig. S3B-E).

Immunohistochemistry

All immunostainings were carried out following protocols described in [20]. Antibodies used in this study: α-Discs large (1:100 DSHB), α-PH3 (1:2000 Cell-Signaling), α-dpERK (1:250 Sigma Aldrich), α-Ct (1:50 DSHB), α-Shotgun (1:50 DSHB), α-Arm (1:100 DSHB), α-Wg (1:50 DSHB), α-Vg (1:200 Gift from Kirsten Guss), α-Twi (1:2000 gift from S. Roth), Phalloidin-iFlor 647 and Phalloidin-iFlor 555 (1:2000 Abcam). Alexa Fluor-conjugated secondary antibodies (1:1000, Thermo Fisher Scientific) were used for immunofluorescence detection.

Mosaic analyses

To generate FLP-out clones of AMPs of various genotypes, females of *hsflp; htl>FRT>stop>FRT>Gal4; UAS-X* flies (*X=UAS-CD8:GFP, UAS-CD8:RFP, UAS-nls:GFP* or *UAS-Lifeact:GFP)* were crossed to w^{1118} (control), *UAS-diaRNAi* (for *dia* knockdown), or *UAS-htlRNAi* (for *htl* knockdown) male flies. Crosses were reared at room temperature and clones were induced by heat shock following standard methods prior to analyses as described in [20].

Electron Microscopy

After careful dissection from larvae, wing discs from w^{1118} larvae were immersed in a fixative mixture of 2.5% glutaraldehyde (GA) and 2.5% paraformaldehyde (PFA) in 0.1M sodium cacodylate buffer, pH 7.4 at room temperature for at least 60 minutes. Buffer washes (0.1M sodium cacodylate) to remove excess initial fixative preceded a 60-minute secondary fixation in 1% osmium tetroxide reduced with 1% ferrocyanide [62] in 0.1M sodium cacodylate buffer. After washing in distilled water, the discs were placed in 2% aqueous uranyl acetate for 60 minutes before dehydrating in an ascending series of ethanol (35% to 100%). The discs were then infiltrated with propylene oxide, low viscosity epoxy resin series before polymerization of the resin at 70°C for 8-12 hours. Thin sections (60-90 nm) were cut from the polymerized blocks with a Reichert-Jung

Ultracut E ultramicrotome, placed on 200 mesh copper grids, and stained with 0.2% lead citrate [63]. Images were recorded at 80 kV on a Hitachi HT7700 transmission electron microscope.

Live imaging of ex vivo cultured wing discs

Long-term live imaging of ex-vivo cultured wing discs was performed using a custom-built 3D-printed imaging chamber following Barbosa and Kornberg [64]. Wing discs were carefully dissected in WM1 media and cultured within a 3D-printed imaging chamber placed over a glass-bottom dish. Wing discs were oriented to face the peripodial side toward the glass-bottom imaging surface for better AMP cytoneme detection deep inside the tissue. Time-lapse movies were captured at one-minute intervals using a 40X oil objective (1.4NA) in a spinning disc confocal microscope.

Light microscopy and image processing

Spinning disc and line-scanning confocal: For most imaging experiments, we used a Yokogawa CSUX1 spinning disc confocal system equipped with an iXon 897 EMCCD camera and Zeiss LSM 900 with Airyscan 2 and GaAsP detectors. Images were resolved using either 20X (0.5NA), 40X (1.3NA oil), 60X (1.4NA oil, Spinning disc), or 63X (1.4NA oil for LSM Airyscan) objectives.

Triple-View line confocal: For deep-tissue high-resolution imaging within a large 3D volume (Fig 3B-D''), we used triple-view line-confocal microscopy as described in [41]. Wing discs of the genotype *ths-Gal4/UAS-nls:mCherry; htl-LexA/ LexO-CD2:GFP* were fixed in 4% PFA, washed 3X with 0.1% PBST, and mounted on a poly-L-lysine-coated coverslip held inside a custom-designed imaging chamber (Applied Scientific Instrumentation, I-2450) with the peripodial side of the discs facing the cover-slip (Fig. 3B). The chamber was mounted onto the microscope stage and filled with 1X PBS prior to imaging. Image volumes were captured using one 60X objective (1.2 NA water immersion lens) beneath the coverslip and two 40X objectives (0.8 NA water dipping lenses) assembled at 90 degrees to each other, imaging the sample from above. All three confocal views were registered and merged with additive deconvolution to

improve axial resolution and recover signals that would otherwise be lost due to scattering [41].

Image processing. All images were processed using Fiji, MATLAB, or Imaris software. The registration and deconvolution of triple-view line confocal images were performed with a custom-written software in MATLAB (MathWorks, R2019b, using the Image Processing and Parallel Computing Toolboxes).

QUANTIFICATION AND STATISTICAL ANALYSIS

Quantitation of cell number

Cell numbers were manually counted from sequential 25μm thick YZ maximum intensity sections visualized in Imaris to cover clones within the entire disc area.

Quantitation of cytonemes numbers, length, and dynamics

Cytonemes were manually counted from the maximum intensity YZ projections derived from 25μm thick YZ sections taken at the center of the disc. For comparative analyses, identical central areas from discs of different genotypes were chosen, and cytoneme counts were normalized per 100 μm using a line drawn along the disc-AMP junction in each YZ section. Cytoneme length represents the length between the base and tip of a cytoneme. Niche occupancy or cytoneme density (Fig 2I) was measured by counting the number of cytonemes at every 5 min interval from a 1400 μm^2 ROI in YZ sections obtained using Imaris. Cytoneme dynamics were measured following [21]. Average extension and retraction rates represent the averaged extension and retraction rates of the observed cytoneme during its respective lifetime. The extension and retraction rate of a given cytoneme represents the positive and negative slope respectively of the experimentally measured cytoneme-length data graph during its lifetime. The lifetime of a cytoneme constitutes the total time for the extension and retraction cycle of a given cytoneme during the period of observation.

Quantitation of cell polarity

The polarity of a cell/nucleus was measured by the angle θ between the major axis of an elliptical cell/nucleus and the disc plane immediately under the cell/nucleus, as shown in Figure 1G.

Quantification of colocalization of Ths:GFP on cytonemes

We used FIJI to derive intensity profiles across Ths:GFP puncta and cytonemes from single XZ and ZY slices and analyzed the profiles for apparent colocalization. Ths:GFP puncta and cytonemes were colocalized to within one pixel (i.e., 97.5 nm) (Fig. S3I,I'). For graphs in Figure S3I-I', fluorescence intensities were normalized to the maximum intensity.

Statistical analyses

Statistical analyses were performed using VassarStat and GraphPad Prism 8. P-values were determined using the unpaired two-tailed t-test for pair-wise comparisons or the ANOVA test followed by Tukey's honestly significant difference (HSD) test for comparison of multiple groups. Differences were considered significant when p-values were <0.05. All measurements were performed from at least three or more wing discs. All graphs and kymographs were generated using GraphPad Prism 8.

Genotypes in Figures

Fig.1. (B-D) *w^{1118}.* (E-K) *UAS-nls:GFP/+; htl-Gal4/+*.

Fig.2. (B-B"') *hs-Flp; UAS-CD8:GFP; htl>FRT>stop>FRT>Gal4*. (C-C') *1151-Gal4/+; UAS-CD8:GFP/+*. (D) *UAS-Lifeact:GFP/UAS-mCherryCAAX; htl-Gal4/+*. (F) *ths-Gal4, UAS-mCherryCAAX/UAS-Lifeact:GFP*, (G,H,I,J) *LexO-CD2:GFP, htl-LexA*. (E; in-order of graphs) (*1151-Gal4/+; UAS-CD8:GFP)*, (*htl-Gal4, UAS-CD8GFP)*, (*UAS-Lifeact:GFP; htl-Gal4)*, (*LexO-mCherryCAAX; htl-LexA)*, (*LexO-CD2:GFP, htl-LexA).*

Fig. 3. (C-D") *ths-Gal4/ UAS-nls:mCherry ; htl-LexA/ LexO-CD2:GFP*. (E-H') *ths-Gal4, UAS-mCherryCAAX/+ ; htl-LexA, LexO-CD2:GFP/+*. (I-I') *UAS-Lifeact:GFP; htl-Gal4*. (J) *htl-LexA, LexO-CD2:GFP*. (K-K') *ths-Gal4/LexO-nsyb:GFP^{1-10}, UAS-CD4:GFP^{11}; htl-LexA/LexO-mCherryCAAX*.

Fig 4. (A) *UAS-mCherryCAAX/UAS-Dia:GFP; htl-Gal4/+*. (B): *hsflp/+; UAS-mCherryCAAX/+; htl>FRT>stop>FRT>Gal4/UAS-Dia^{act}:GFP*. (C,E) *UAS-Lifeact:GFP/+, htl-Gal4/+*. (D,F-G') *UAS-Lifeact:GFP/+, htl-Gal4/UAS-diaRNAi*. (H-H') *UAS-nls:GFP/+; htl-Gal4/+*, (I-I'): *UAS-nls:GFP/+ ; htl-Gal4/UAS-diaRNAi*. (J-K') *HS-Flp/+; UAS-Lifeact:GFP/+; htl>FRT>stop>FRT>Gal4/+*. (L-O) *HS-Flp/+; UAS-Lifeact:GFP/+; htl>FRT>stop>FRT>Gal4/UAS-diaRNAi*.

Fig. 5. (A) *LexO-Fz:mCherry/+*; *htl-LexA*, *LexO-CD2:GFP/+*. (B): *LexO-Htl:mCherry/+*; *htl-LexA*, *LexO-CD2:GFP/+.* (D) *htl:GFP^{fTRG}*. (E-F") *HS-Flp/+; UAS-CD8:RFP/+; htl>FRT>stop>FRT>Gal4/+*. (G-G') *HS-Flp/+; UAS-CD8:RFP/UAS-htlRNAi; htl>FRT>stop>FRT>Gal4/+*. (H-H") *UAS-Lifeact:GFP/UAS-htlRNAi, htl-Gal4/+*. (K-K"): *UAS-nls:GFP/UAS-htlRNAi, htl-Gal4/+*. (I) *HS-Flp/+; UAS-Lifeact:GFP/UAS-htlRNAi; htl>FRT>stop>FRT>Gal4/+*. (M) *HS-Flp/+; UAS-nls:GFP/+; htl>FRT>stop>FRT>Gal4/+*. (M') *HS-Flp/+; UAS-nls:GFP/UAS-htlRNAi; htl>FRT>stop>FRT>Gal4/+*.

Fig. 6. (A) *ths-Gal4, UAS-mCherryCAAX/+; htl-LexA, LexO-CD2:GFP/+*. (C) *pyr-Gal4/+; UAS-CD8:GFP/+*. (D) *pyr-Gal4, UAS-mCherryCAAX/+; htl-LexA, LexO-CD2:GFP/+*, (E,G) *ths-Gal4/+; UAS-CD8GFP/+*. (F,H): *pyr-Gal4/+; UAS-CD8GFP/+*, (K,K'): *ths-Gal4, UAS-mCherryCAAX/+; htl-LexA, LexO-CD2:GFP/+.* (J,L,L',M-M") *ths-Gal4, UAS-mCherryCAAX/+; htl-LexA, LexO-CD2:GFP/UAS-thsRNAi*. (N-N'''): *pyr-Gal4, UAS-mCherryCAAX/+; htl-LexA, LexO-CD2:GFP/+*. (O-P'): *pyr-Gal4, UAS-mCherryCAAX/UAS-pyrRNAi; htl-LexA, LexO-CD2:GFP/+*.

Fig. 7. (A-A") *ths-Gal4, UAS-mCherryCAAX/UAS-Ths:GFP*. (B-B') *pyr-Gal4, UAS-mCherryCAAX/+; UAS-Pyr:GFP/+*. (C,G-H') *ths-Gal4/LexO-mCherryCAAX; htl-LexA/UAS-Ths:GFP*. (D,D',I-I") *pyr-Gal4/LexO-mCherryCAAX; htl-LexA/UAS-Pyr:GFP*. (E) *ths-Gal4/LexO-nls:mCherry; htl-LexA/UAS-Ths:GFP*. (F-F') *pyr-Gal4/LexO-nls:mCherry; htl-LexA/UAS-Pyr:GFP.*

Fig. 8 (B-B') *dpp-Gal4, UAS-mCherryCAAX/+*, (C,D) *dpp-Gal4, UAS-mCherryCAAX/+; UAS-Pyr:GFP/+*. (E,F) *dpp-Gal4, UAS-mCherryCAAX/UAS-Ths:GFP*. (G-G"') *dpp-Gal4/LexO-mCherryCAAX; htl-LexA/UAS-Ths:GFP*.

SUPPLEMENTAL INFORMATION

Tables S1-S4

Figures S1-S3

Videos S1-S8

REFERENCES

1. Yamashita, Y. M., Yuan, H., Cheng, J. & Hunt, A. J. Polarity in stem cell division: asymmetric stem cell division in tissue homeostasis. *Cold Spring Harbor Perspectives in Biology* **2,** a001313 (2010).
2. Losick, V. P., Morris, L. X., Fox, D. T. & Spradling, A. Drosophila Stem Cell Niches: A Decade of Discovery Suggests a Unified View of Stem Cell Regulation. *Developmental Cell* **21,** 159–171 (2011).
3. Florian, M. C. & Geiger, H. Concise review: polarity in stem cells, disease, and aging. *Stem Cells* **28,** 1623–1629 (2010).
4. Morrison, S. J. & Spradling, A. C. Stem Cells and Niches: Mechanisms That Promote Stem Cell Maintenance throughout Life. *Cell* **132,** 598–611 (2008).
5. Venkei, Z. G. & Yamashita, Y. M. Emerging mechanisms of asymmetric stem cell division. *J Cell Biol* **217,** 3785–3795 (2018).
6. Nystul, T. G. & Spradling, A. C. Breaking out of the mold: diversity within adult stem cells and their niches. *Current Opinion in Genetics & Development* **16,** 463–468 (2006).
7. Li, L. & Xie, T. Stem cell niche: structure and function. *Annu. Rev. Cell Dev. Biol.* **21,** 605–631 (2005).
8. Zhang, J. & Li, L. Stem cell niche: microenvironment and beyond. *Journal of Biological Chemistry* **283,** 9499–9503 (2008).
9. Rompolas, P., Mesa, K. R. & Greco, V. Spatial organization within a niche as a determinant of stem-cell fate. *Nature* **502,** 513–518 (2013).
10. Yu, F., Kuo, C. T. & Jan, Y.-N. Drosophila neuroblast asymmetric cell division: recent advances and implications for stem cell biology. *Neuron* **51,** 13–20 (2006).
11. Yamashita, Y. M., Fuller, M. T. & Jones, D. L. Signaling in stem cell niches: lessons from the Drosophila germline. *Journal of Cell Science* **118,** 665–672 (2005).
12. Buszczak, M., Inaba, M. & Yamashita, Y. M. Signaling by Cellular Protrusions: Keeping the Conversation Private. *Trends Cell Biol.* **26,** 526–534 (2016).
13. Habib, S. J. *et al.* A localized Wnt signal orients asymmetric stem cell division in vitro. *Science* **339,** 1445–1448 (2013).
14. Ramírez-Weber, F. A. & Kornberg, T. B. Cytonemes: cellular processes that project to the principal signaling center in Drosophila imaginal discs. *Cell* **97,** 599–607 (1999).
15. Roy, S., Huang, H., Liu, S. & Kornberg, T. B. Cytoneme-mediated contact-dependent transport of the Drosophila decapentaplegic signaling protein. *Science* **343,** 1244624–1244624 (2014).

16. Kornberg, T. B. & Roy, S. Communicating by touch--neurons are not alone. *Trends Cell Biol.* **24,** 370–376 (2014).
17. Roy, S., Hsiung, F. & Kornberg, T. B. Specificity of Drosophila Cytonemes for Distinct Signaling Pathways. *Science* **332,** 354–358 (2011).
18. Bischoff, M. *et al.* Cytonemes are required for the establishment of a normal Hedgehog morphogen gradient in Drosophila epithelia. *Nat Cell Biol* **15,** 1269–1281 (2013).
19. Stanganello, E. & Scholpp, S. Role of cytonemes in Wnt transport. *Journal of Cell Science* **129,** 665–672 (2016).
20. Du, L., Sohr, A., Yan, G. & Roy, S. Feedback regulation of cytoneme-mediated transport shapes a tissue-specific FGF morphogen gradient. (2018). doi:10.7554/eLife.38137
21. Du, L., Sohr, A. & Roy, S. GPI-anchored FGF directs cytoneme-mediated bidirectional signaling to self-regulate tissue-specific dispersion. *bioRxiv* 2021.02.23.432493 (2021).
22. Hall, E. T. *et al.* Cytoneme delivery of Sonic Hedgehog from ligand-producing cells requires Myosin 10 and a Dispatched-BOC/CDON co-receptor complex. *Elife* **10,** (2021).
23. Kornberg, T. B. & Roy, S. Cytonemes as specialized signaling filopodia. *Development* **141,** 729–736 (2014).
24. Zhang, C. & Scholpp, S. Cytonemes in development. *Current Opinion in Genetics & Development* **57,** 25–30 (2019).
25. González-Mendez, L., Gradilla, A.-C. & Guerrero, I. The cytoneme connection: direct long-distance signal transfer during development. *Development* **146,** dev174607 (2019).
26. Rojas-Rios, P., Guerrero, I. & Gonzalez-Reyes, A. Cytoneme-mediated delivery of hedgehog regulates the expression of bone morphogenetic proteins to maintain germline stem cells in Drosophila. *PLoS Biol* **10,** e1001298–13 (2012).
27. Inaba, M., Buszczak, M. & Yamashita, Y. M. Nanotubes mediate niche-stem-cell signalling in the Drosophila testis. *Nature* **523,** 329–332 (2015).
28. Junyent, S. *et al.* Specialized cytonemes induce self-organization of stem cells. *Proc. Natl. Acad. Sci. U.S.A.* **117,** 7236–7244 (2020).
29. Fernandes, J., Bate, M. & VijayRaghavan, K. Development of the indirect flight muscles of Drosophila. *Development* **113,** 67–77 (1991).
30. Gunage, R. D., Reichert, H. & VijayRaghavan, K. Identification of a new stem cell population that generates Drosophila flight muscles. *Elife* **3,** (2014).
31. Bate, M., Rushton, E. & Currie, D. A. Cells with persistent twist expression are the embryonic precursors of adult muscles in Drosophila. *Development* **113,** 79–89 (1991).
32. Roy, S. & VijayRaghavan, K. Muscle pattern diversification in Drosophila: the story of imaginal myogenesis. *Bioessays* **21,** 486–498 (1999).
33. Sudarsan, V., Anant, S., Guptan, P., VijayRaghavan, K. & Skaer, H. Myoblast diversification and ectodermal signaling in Drosophila. *Developmental Cell* **1,** 829–839 (2001).
34. Gunage, R. D., Dhanyasi, N., Reichert, H. & VijayRaghavan, K. Drosophila adult muscle development and regeneration. *Semin. Cell Dev. Biol.* **72,** 56–66 (2017).

35. Vishal, K., Lovato, T. L., Bragg, C., Chechenova, M. B. & Cripps, R. M. FGF signaling promotes myoblast proliferation through activation of wingless signaling. *Dev. Biol.* **464,** 1–10 (2020).
36. Huang, H. & Kornberg, T. B. Myoblast cytonemes mediate Wg signaling from the wing imaginal disc and Delta-Notch signaling to the air sac primordium. *Elife* **4,** e06114 (2015).
37. Wood, B. M. *et al.* Cytonemes with complex geometries and composition extend into invaginations of target cells. *J Cell Biol* **220,** (2021).
38. Sato, M. & Kornberg, T. B. FGF is an essential mitogen and chemoattractant for the air sacs of the drosophila tracheal system. *Developmental Cell* **3,** 195–207 (2002).
39. Abmayr, S. M. & Pavlath, G. K. Myoblast fusion: lessons from flies and mice. *Development* **139,** 641–656 (2012).
40. Anant, S., Roy, S. & VijayRaghavan, K. Twist and Notch negatively regulate adult muscle differentiation in Drosophila. *Development* **125,** 1361–1369 (1998).
41. Wu, Y. *et al.* Multiview super-resolution microscopy. *bioRxiv* 2021.05.21.445200 (2021).
42. Macpherson, L. J. *et al.* Dynamic labelling of neural connections in multiple colours by trans-synaptic fluorescence complementation. *Nat Comms* **6,** 10024 (2015).
43. Deng, S., Bothe, I. & Baylies, M. K. The Formin Diaphanous Regulates Myoblast Fusion through Actin Polymerization and Arp2/3 Regulation. *PLoS Genet* **11,** e1005381 (2015).
44. Everetts, N. J., Worley, M. I., Yasutomi, R., Yosef, N. & Hariharan, I. K. Single-cell transcriptomics of the Drosophila wing disc reveals instructive epithelium-to-myoblast interactions. *Elife* **10,** (2021).
45. Sarov, M. *et al.* A genome-wide resource for the analysis of protein localisation in Drosophila. *Elife* **5,** e12068 (2016).
46. Stathopoulos, A., Tam, B., Ronshaugen, M., Frasch, M. & Levine, M. pyramus and thisbe: FGF genes that pattern the mesoderm of Drosophila embryos. *Genes & Development* **18,** 687–699 (2004).
47. Losick, V. P., Morris, L. X., Fox, D. T. & Spradling, A. Drosophila Stem Cell Niches: A Decade of Discovery Suggests a Unified View of Stem Cell Regulation. *Developmental Cell* **21,** 159–171 (2011).
48. Segal, D., Dhanyasi, N., Schejter, E. D. & Shilo, B.-Z. Adhesion and Fusion of Muscle Cells Are Promoted by Filopodia. *Developmental Cell* **38,** 291–304 (2016).
49. Aradhya, R., Zmojdzian, M., Da Ponte, J. P. & Jagla, K. Muscle niche-driven Insulin-Notch-Myc cascade reactivates dormant Adult Muscle Precursors in Drosophila. *Elife* **4,** (2015).
50. Stepanik, V., Sun, J. & Stathopoulos, A. FGF Pyramus Has a Transmembrane Domain and Cell-Autonomous Function in Polarity. *Curr. Biol.* (2020). doi:10.1016/j.cub.2020.06.006.
51. Mossahebi-Mohammadi, M., Quan, M., Zhang, J.-S. & Li, X. FGF Signaling Pathway: A Key Regulator of Stem Cell Pluripotency. *Front Cell Dev Biol* **8,** 79 (2020).

52. Huang, Y. *et al.* Type 2 Fibroblast Growth Factor Receptor Signaling Preserves Stemness and Prevents Differentiation of Prostate Stem Cells from the Basal Compartment. *J. Biol. Chem.* **290,** 17753–17761 (2015).
53. Roth, S., Stein, D. & Nüsslein-Volhard, C. A gradient of nuclear localization of the dorsal protein determines dorsoventral pattern in the Drosophila embryo. *Cell* **59,** 1189–1202 (1989).
54. Williams, J. A., Bell, J. B. & Carroll, S. B. Control of Drosophila wing and haltere development by the nuclear vestigial gene product. *Genes & Development* **5,** 2481–2495 (1991).
55. Port, F., Chen, H. M., Lee, T. & Bullock, S. L. *An optimized CRISPR/Cas toolbox for efficient germline and somatic genome engineering in Drosophila*. (2014). doi:10.1101/003541
56. Pfeiffer, B. D. *et al.* Tools for neuroanatomy and neurogenetics in Drosophila. *Proc. Natl. Acad. Sci. U.S.A.* **105,** 9715–9720 (2008).
57. Du, L. *et al.* Unique patterns of organization and migration of FGF-expressing cells during Drosophila morphogenesis. *Dev. Biol.* **427,** 35–48 (2017).
58. Gratz, S. J. *et al.* Highly specific and efficient CRISPR/Cas9-catalyzed homology-directed repair in Drosophila. *Genetics* **196,** 961–971 (2014).
59. Du, L., Zhou, A., Sohr, A. & Roy, S. An Efficient Strategy for Generating Tissue-specific Binary Transcription Systems in Drosophila by Genome Editing. *J Vis Exp* (2018). doi:10.3791/58268
60. Stathopoulos, A., Tam, B., Ronshaugen, M., Frasch, M. & Levine, M. pyramus and thisbe: FGF genes that pattern the mesoderm of Drosophila embryos. *Genes & Development* **18,** 687–699 (2004).
61. Yang, S. *et al.* FGF signaling directs myotube guidance by regulating Rac activity. *Development* **147,** (2020).
62. Rivlin, P. K. & Raymond, P. A. Use of osmium tetroxide-potassium ferricyanide in reconstructing cells from serial ultrathin sections. *J. Neurosci. Methods* **20,** 23–33 (1987).
63. VENABLE, J. H. & COGGESHALL, R. A SIMPLIFIED LEAD CITRATE STAIN FOR USE IN ELECTRON MICROSCOPY. *J Cell Biol* **25,** 407–408 (1965).

64. Barbosa GO, Kornberg TB. *ex vivo* time lapse imaging of *Drosophila melanogaster* cytonemes [submitted].